Doctoral Dissertation (Shinshu University)

Synthesis of Chemically-Derived Graphene Electrodes

for Electrochemical Capacitor Application

Sep 2014

Zhongwei LEI

Contents

Chapter 1

General Introduction

1.1 Electrochemical capacitor

1.1.1 General introduction

Electrochemical capacitors, also known as electric doube-layer capacitors (EDLC), supercapacitors or ultracapacitors, store electrical charge in the electrical double layer at the electrode-electrolyte interface.[1,2] Electrochemical capacitors are able to store much more charge compared to conventional capacitors, allowing usage for energy storage. The physical adsorption/desorption of ions at the electrode-electrolyte interface gives electrochemical capacitors very high power density compared to other energy storage devices such as batteries or fuel cells. Figure 1-1 shows a rough comparison of energy
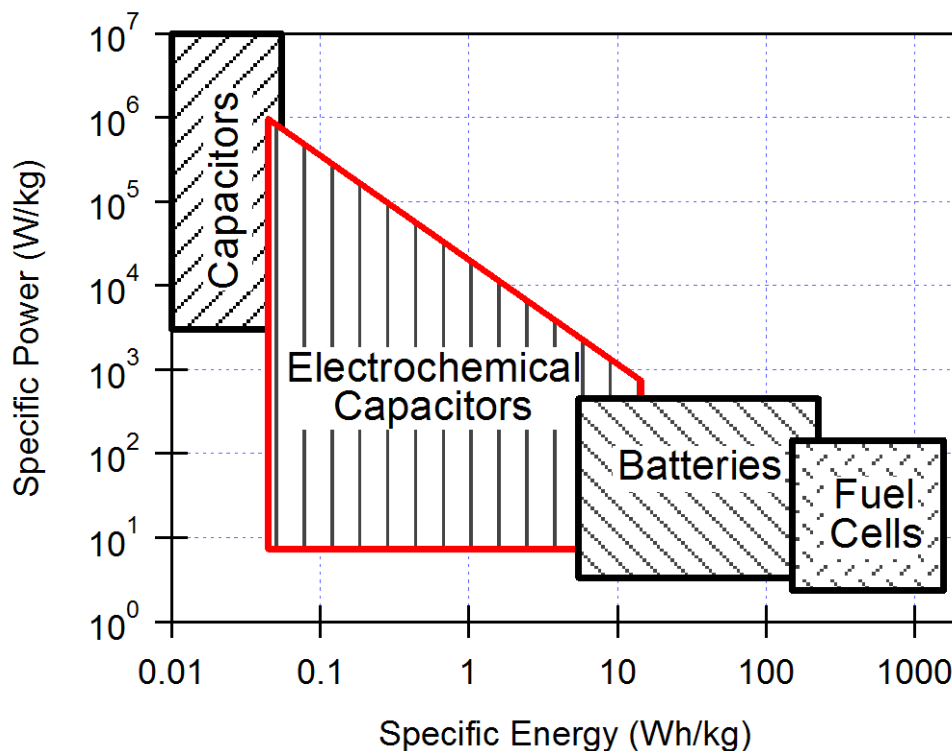

Figure 1-1. Ragone plot showing the rough comparison for various energy storage devices. (Re-produced from ref. 2)

and power density for different energy storage systems. Electrochemical capacitors fill the gap between batteries and traditional capacitors in terms of energy density and power density. Batteries and fuel cells have high energy density but cannot provide high power, while conventional capacitors such as electrolytic capacitors or metalized film capacitors provide high power at very low energy density. In addition, owning to the charge/discharge process without chemical reactions, electrochemical capacitors can be fully charged in seconds to minutes compared to hours for batteries. Electrochemical capacitors also have much longer cycle life (>100,000 cycles) than batteries (~3000 cycles for Li-ion batteries for example).[1-4] Owing to these properties, electrochemical capacitors have successfully found application in uninterruptable power supplies (UPS), portable electronics, toys, solar watches and so on, and has been introduced in electric vehicles (EV) or hybrid electric vehicles (HEV), where they can make use of their features of fast charging (harvesting of braking energy) and high power (starting).[2-6]

1.1.2 Brief history

The concept of storing charge in the electrical double layer at the electrode-electrolyte interface has been known since 1800s. Several patents[7, 8] were granted for the design of electrical double layer based capacitors, the first practical electrochemical capacitor was not introduced until 1970.[9] NEC first introduced electrochemical capacitors commercially as a *Supercapacitor*® in 1978, under license from SOHIO. As electrochemical capacitors were applied in more and more fields, a

number of manufacturers around the world introduced their products in different commercial names, for example, *PSCap* from ECOND, *Goldcap* from Panasonic, *DLCAP*^{TM} from Nippon Chemi-con, *Dynacap* from Elna, *Ultracapacitor* from Maxwell.

1.1.3 Basic principles of electrochemical capacitors

For a conventional capacitor (Figure 1-2), two metal plates with the same area of A are separated by a dielectric of thickness of d. Then the capacitance C of the capacitor is defined as:

$$C = \frac{Q}{V} \tag{1-1}$$

Where Q is the accumulated charge on each plate and V is the potential difference between the two plates. C is determined by the dimension of the capacitor and the property of dielectric between the plates, and can be calculated by:

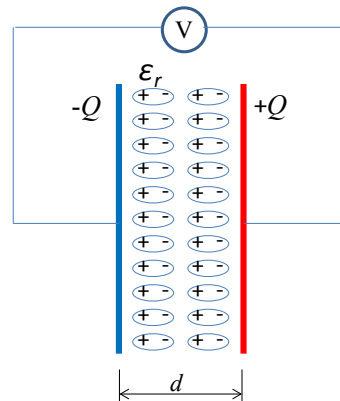$$C = \varepsilon_0 \varepsilon_r A / d \tag{1-2}$$

Figure 1-2. Schematic for a capacitor with two parallel conductive plates.

Where ε_0 is the permittivity in vacuum and ε_r is the relative dielectric constant of

the dielectric between the charged plates.
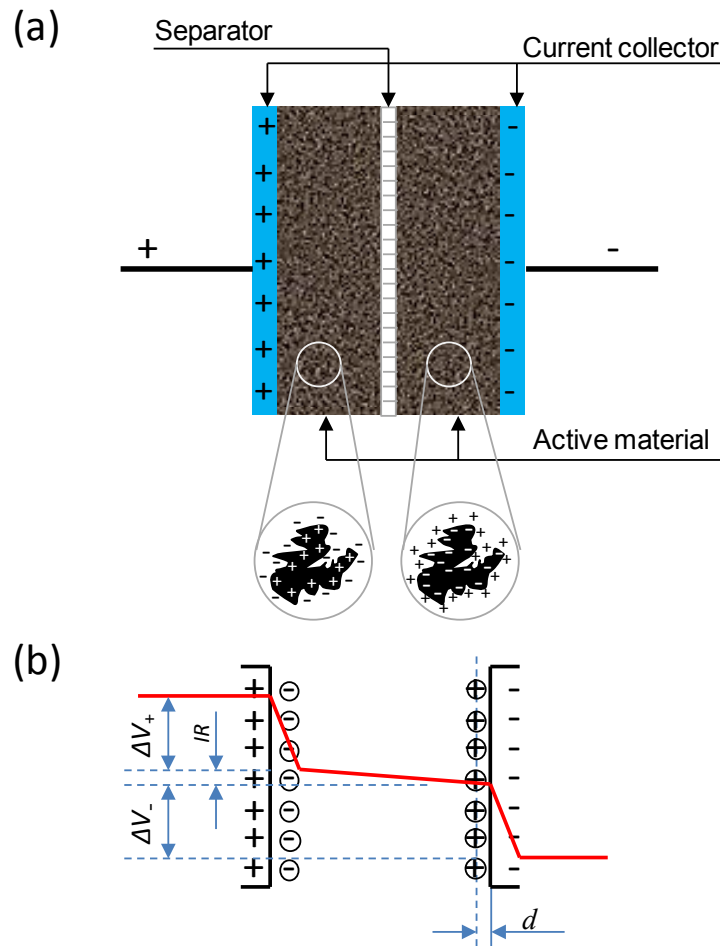
Figure 1-3. (a) Basic structure of an electrochemical capacitor, and (b) illustration of potential drop at the electrode/electrolyte interface.[2]

In the case of an electrical double-layer capacitor, as shown schematically in Figure 1-3,[2] the two charged plates are replaced by the so called "electrical double layer" which is composed of a charged solid surface (typically activated carbon) and a compact layer of ions with opposite charge in electrolyte. The double layer thickness d is typically 0.5 nm to 1 nm, depending on the size of ions and solvent molecules, and

the concentration of electrolyte. Because of the extremely thin separation gap between the opposite charge layers, the corresponding electric field across the electrode-electrolyte interface is extremely high and assumed to be up to 10^6-10^8 V cm^{-1},[1] with the relative dielectric constant $\bullet_r$ of ~10 for water or lower for organic solvents,[10] the specific capacitance can reach values of 20-50 μF cm^{-2} for a typical electrical double layer.[2]

For an ideal battery, when it is discharged or recharged, the potential will be kept at an almost constant value As shown in Figure 1-4. While for an ideal capacitor, the potential is proportional to its state of charge because $Q=CV$, where C is constant. The energy stored in an ideal capacitor is:

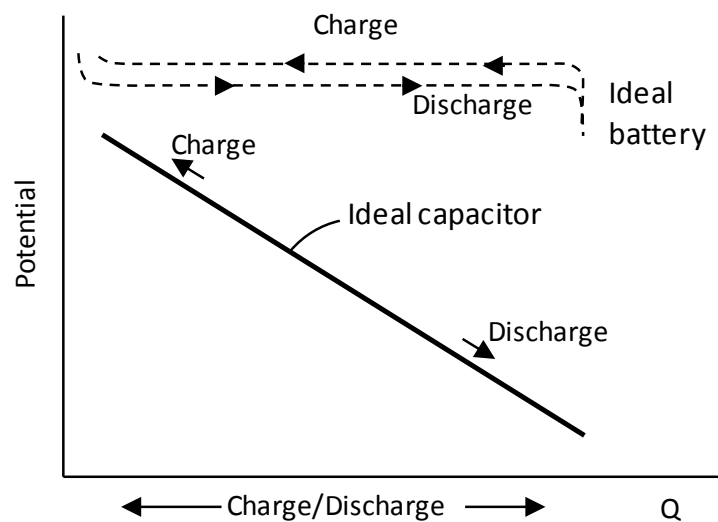$$E = \frac{1}{2}CV^2 \qquad\qquad (1\text{-}3)$$

Figure 1-4. Comparison of charge/discharge behavior of a typical capacitor and a typical battery.

The cell voltage influences the energy storage most, and is limited by the electrochemical decomposition of the solvent of the electrolyte. Thus, aqueous systems have cell voltage typically lower than 1.2 V. Most commercial electrochemical capacitors today use organic solvents such as polyethylene carbonate (PC) or acetonitrile (AN) as the electrolyte by which the cell voltage can be extended to 2-3 V, giving typical energy density of ~5 Wh kg^{-1}.[1] However, this is still far from ~120 Wh kg^{-1} for Li-ion batteries, leaving a large space for improvement of this promising device.

Psuedo-capacitor (or redox capacitor) is also known as a type of electrochemical capacitor, which utilizes fast reversible reactions in addition to the electrical double layer capacitance for the energy storage.[1] It usually improves the energy density of electrochemical capacitors at the cost of power density and life time in some extent due to the relatively slow kinetics of the redox (chemical) reaction compared to the pure adsorption/desorption (physical) process.

1.2 Electrode materials for electrochemical capacitors

Based on the principle of electrochemical capacitors, some key requirements for the electro-active material can be summarized as follows:

- ⊕ High specific surface area with open porosity
- ⊕ High electronic conductivity
- ⊕ Good wettability to electrolyte
- ⊕ Good electrochemical stability

✧ Low cost and good processability

Activated carbon (AC) is the electrode material used in most commercial electrochemical capacitors currently, possessing high specific surface area (typically 500-2000 m^2 g^{-1}, the highest can be over 3000 m^2 g^{-1}), good chemical stability, at a relatively low cost. However, the electronic conductivity of activated carbon is not sufficient, therefore, 5-10% of carbon black is necessary to be added as a conductive additive in the typical process of commercial electrochemical capacitors. Research on other materials as well as the improvement of AC is being intensively conducted.

The pore size of the active material is regarded to be one of the key factors to its specific capacitance. It was conventionally considered that the porosities with too small size (with diameter below 0.5 nm or even 1 nm) cannot contribute to capacitive charge storage because they are inaccessible to solvated ions, especially in the case of organic electrolytes. Thus, a pore size in the range of 2-5 nm, which is larger than 2 times of the size of a typical solvated ion, was expected to be desirable for the application in electrochemical capacitors. However, recent studies show that as the pore size goes down to less than 1 nm (typically ~0.7 nm), the specific capacitance increases dramatically as the pore size decreases (Figure 1-5).[11, 12] Carbide-derived carbon (CDC) with pores of the same size of ions in the electrolyte was reported to show maximum specific capacitance.[13] Theoretical studies suggest that the solvated shells of ions can be removed partially when entering ultra-small micropores.[11] The sudden increase of specific capacitance for pore size smaller than ~1 nm has been attributed to the removal

of co-ions (the ions with same charge with the electrode).

Improvement of activated carbons and other carbon-based materials are also being studied for EC applications, such as,[14-31] carbon nanotube (CNT),[32-34] fullerene[35] and graphene, which will be introduced in detail later.

A number of recent studies have focused on pseudo-capacitive materials, mainly metal oxides (RuO_2, Fe_2O_3, MnO_2, etc.)[36-45] and conductive polymers (polyaniline, polypyrrole, polythiophene and their derivatives)[46-48]. These materials usually show higher specific capacitance than pure electrical double layer capacitors, but often suffer from low cell voltage and/or poor cycleability.
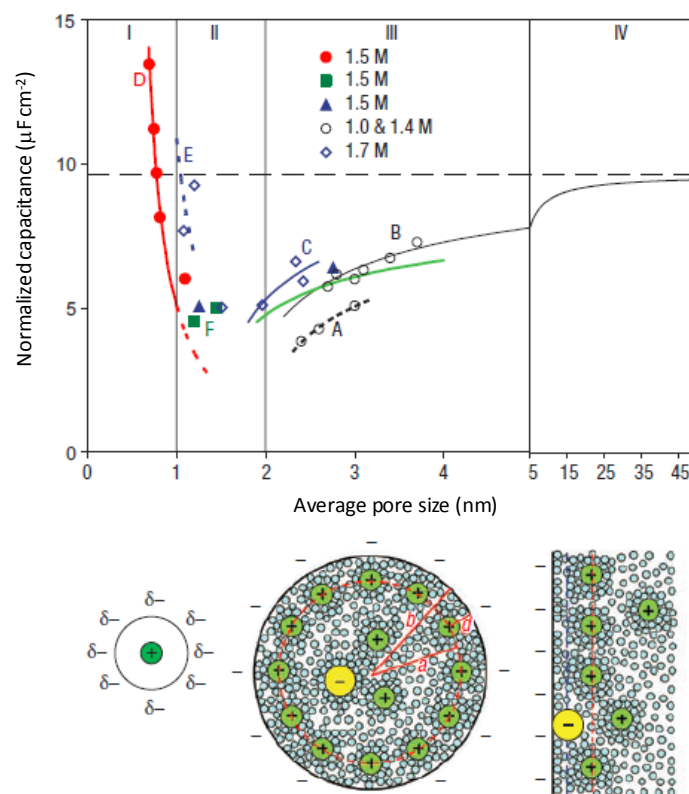

Figure 1-5 Specific capacitance normalized by surface area as a function of the pore size for different carbon samples. Reprinted from ref. 12.

1.3 Graphene: a promising candidate for electrode material of electrochemical capacitors
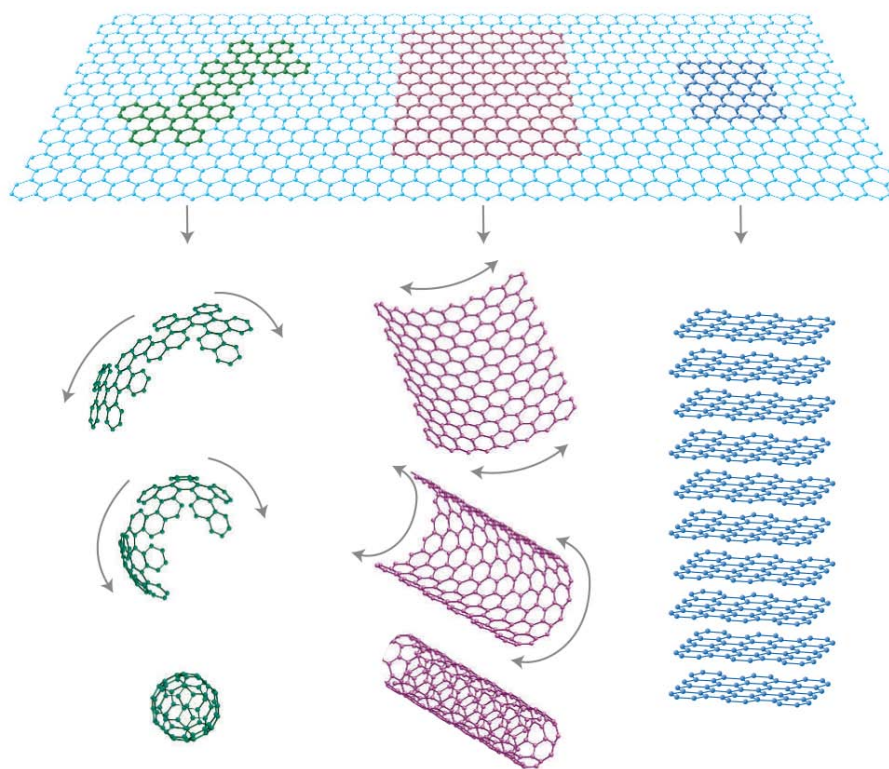
Figure 1-7. Schematic of grahene as the mother of all graphitic materials.[55]

Graphene is a 2-dimensional crystal with a monolayer of carbon atoms tightly packed into a honeycomb lattice. It is the basic building block for all graphitic materials such as fullerene, carbon nanotube or graphite (Figure 1-7).[51] Isolated graphene was presumed to be not able to exist at ambient condition because of thermal fluctuation. In 2004, A. K. Geim and K. S. Novoselov reported the successful isolation of graphene using adhesive tape,[49] initiating a world-wide search for extraordinary properties of the

thinnest crystal had even found.[52-57]

1.3.1 Properties of graphene

Carbon atoms in graphene are bond with each other by sp^2 hybrid bonding with a bond length of ~0.142 nm, which is one of the strongest bonds in an material. This makes graphene one of the strongest materials, with a tensile strength over 100 times greater than steel. Theoretically, graphene should posses a specific surface area of 2630 $m^2 g^{-1}$.

Graphene has extraordinary high electron mobility at ambient conditions (~200,000 $cm^2 V^{-1} s^{-1}$).[55] Electrons travel through the graphene sheets as zero-mass, as fast as 1/100 that of the speed of light, which makes it a great conductor, with conductivity better than copper.[55] Also, graphene has very high thermal conductivity of > 5000 $W m^{-1} K^{-1}$,[56] which is much higher than common metals.

The edge of graphene has been shown to be more reactive than the basal plane. However, unless exposed to extremely harsh reaction conditions, graphene is a fairly inert material, and does not react readily despite all atoms being exposed to the surroundings.

1.3.2 Preparation of graphene

A number of approaches have been developed for the preparation of graphene since it was experimentally proven to stably exist under ambient conditions. Mechanical

cleavage of graphite is used to prepare high quality samples in laboratory scale for fundamental studies.[57] However, this method can only prepare samples in mm-scale size and should be difficult to produce at industrial scale. Epitaxial growth on metal substrates such as Ni, Ir or Cu is used for preparation of graphene with larger lateral size.[58-60] Single layer graphene in meter-scale have been successfully prepared by this approach.[59] Graphene can also be prepared by controlled thermal treatment of metal carbides which removes the metal atoms on the surface.[61] The most extensively studied approach for production of graphene is the chemical method via reduction of exfoliated graphite oxide nanosheets, due to the readily scalable procedure and the relative low cost.[51, 62-67]

1.3.3 Research status of graphene-based material as electrode material for electrochemical capacitors

Based on the measured specific capacitance of ~21 μF cm^{-2} [68] and its theoretical specific surface area, a theoretical specific capacitance of ~550 F g^{-1} is expected, which is ~5 times that of activated carbons commonly used today.[1] A perfect monolayer graphene shows a V-shaped specific capacitance curve with respect to a gate potential (Figure 1-8), with a non-zero minimum at the Dirac point and a linear increase on both sides of the minimum.[68] However, since the chemical method via reduction of graphene oxide introduces a large number of defects or impurities into the honeycomb lattice, the ideal V-shape was not reported to be observed for chemically derived graphene.
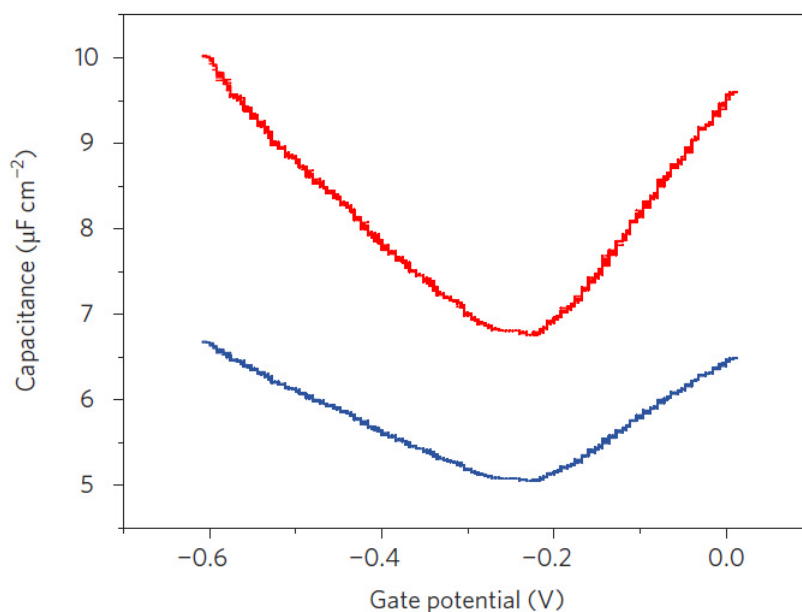
Figure 1-8. Quantum capacitance (red line) and total capacitance (blue line) of monolayer graphene as a function of gate potential,. [68]

A number of studies have been reported using graphene or graphene-based composites as active materials for electrochemical capacitors. Table 1 summarizes the typical values of specific capacitance as well as their preparation methodologies reported in recent years.

Table 1. Summary of typical reported studies of graphene or graphene-based composites for electrochemical capacitor application (SSA: Specific surface area)

Material	Methodology	SSA (m^2/g)	Capacitance (F/g^{-1})	Electrolyte	Ref.
rGO	Thermal reduction	925	115	H_2SO_4	69
rGO	N_2H_4-reduction	705	135	KOH	70
rGO	N_2H_4-reduction	320	205	KOH	71
rGO	Thermal reduction in vaccum	~400	264	KOH	72
rGO	Microwave exfoliation	463	191	5 M KOH	75

rGO	Thermal reduction in PC	--	120	$TEABF_4$/PC	74
PANI/rGO	Liquid mixing	--	210	1 M H_2SO_4	75
Curved rGO	fluidized-bed drying	500	154	Ionic liquid	76
MnO_2/rGO		--	216	1 M Na_2SO_4	77
CB/rGO	Ultrasonic mixing	586	175	6 M KOH	78
Vertical aligned graphene	Plasma-enhanced CVD	--	--	KOH	79
rGO hydrogel	Hydrothermal reduction	951	220	5 M KOH	80
MnO_2/rGO	N_2H_4-reduced GO +Anodic deposited MnO_2	--	328	1 M KCl	81
Activated rGO	KOH-activation of rGO	3100	166	(BMIM BF_4)/AN	82
rGO	Laser reduction of GO	1520	265	($TEABF_4$)/AN	83
B-doped rGO	Borane reduction of GO	466	200	6 M KOH	84
Smaller rGO	Ultrasonic treatment and H_2 reduction	293	242	H_2SO_4	85

From the above as well as a number of other reports, most of the graphite oxide-derived graphene materials for electrochemical capacitor application are prepared by thermal reduction (heat treatment at ~300 °C or thermal shock at ~900 °C) or chemical reduction using hydrazine. New reduction methods such as microwave irradiation[73], laser-scribing[83], or using other chemicals like HI[86], UV irradiation[87], and so on, are being pursued. The specific capacitance of graphene or graphene-like materials derived from graphite oxide reported without combining with other pseudo-capacitive materials ranges between ~30 and over 260 F g^{-1}, a rather wide range. The commonly accepted specific capacitance for graphene ranges from 100-200 F g^{-1}, with slightly lower values in organic electrolytes or ionic liquids. Even with the highest value of 265 F g^{-1} for pure reduced graphite oxide nanosheets fabricated by laser treatment,[83] the specific capacitance of graphene reaches only less than a half of its theoretical value (~550 F g^{-1}).

In 2008, the first attempt was reported to fabricate a graphene-based electrochemical capacitor.[70] Graphene aggregates were prepared by reduction of graphene oxide in liquid phase by hydrazine. Specific capacitance of 135 and 95 F g^{-1} were obtained in aqueous KOH and organic TEABF$_4$/PC electrolytes, respectively. Although a good electronic conductivity and near ideal rectangular shape of cyclic voltammogram were obtained in this first study, due to serious aggregation (aggregated particles with a diameter of ~10 μm), only the graphene sheets near the surface of the aggregates were utilized. Thus the specific capacitance obtained was not so advantageous to conventional activated carbons. Attempts to suppress the restacking of sheets during processing (especially the reduction process) have been conducted. Recently, a 3-D network nanostructure of pillared graphene proposed for hydrogen storage (adsorbing hydrogen molecules on the surface of the pillared graphene),[88] which is similar for that to be used as an electrode for electrochemical capacitor. Based on the theoretical calculation by the authors, the proposed pillared structure (Figure 1-9) with interlayer distance of ~1.2 nm could store ~80% higher hydrogen compare to conventional materials. Functionalization of graphene sheets with various pillars and/or pseudo-capacitive materials like RuO$_2$, TiO$_2$ and Fe$_3$O$_4$ were reported to achieving high specific capacitance.[89] Also, organic material was used to pillar the graphene sheet with hierarchical structure, give a high capacity up to 1600 mAh g^{-1}.[90] A sponge-like graphene nanoarchitecture with highly curved graphene sheets was reported to posses
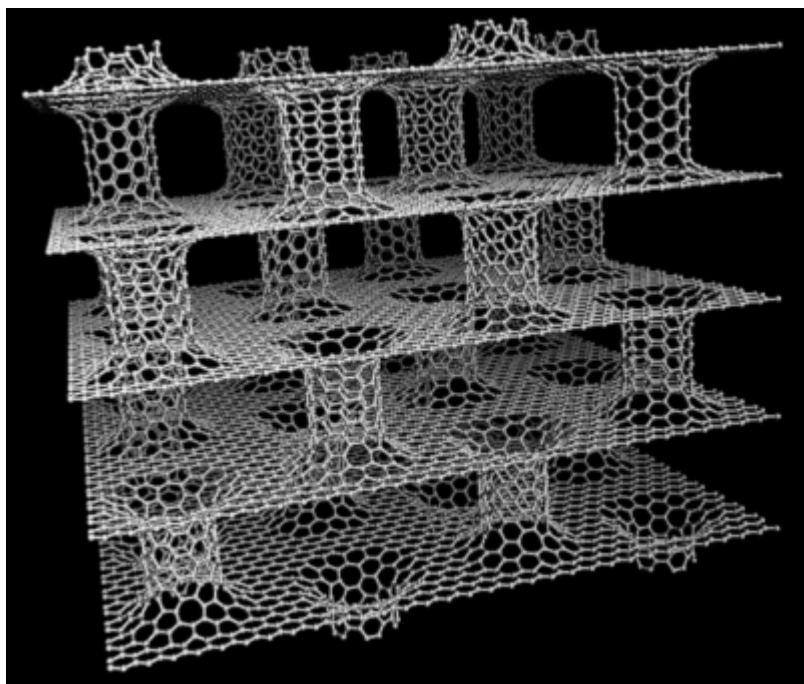
Figure 1-9 Pillared graphene nanostructure proposed by Dimitrakakis et al.[88]

ultrahigh power density up to 48,000 W kg^{-1}.[91]

Plasma-enhanced CVD was employed to prepare vertically aligned graphene sheets directly on metal current collector. Such electrodes can reduce the resistance thereby enhancing the capacitive performance at high frequency (120 Hz).[79] Graphene-based material produced by laser irradiation of graphite oxide coated on metal current collector was reported.[83] The graphene oxide sheets stacked will be reduced and exfoliated simultaneously and form a nano-sponge-like material. This material shows a specific surface area of up to 1520 m^2 g^{-1} and excellent electrochemical capacitive performance in both aqueous and organic electrolytes. Furthermore, this approach directly coat the graphite oxide slurry on metal current collector before reduction,

leading to a good contacting of the active material to the current collector without the presence of binder, as a result, this material shows much higher power density compared to conventional ECs with activated carbon. This method was reported to be used for fabrication of micro-supercapacitors.[92]

Summarizing the recent literatures, a number of factors can be considered to significantly affect the specific capacitance of graphene:

a. Face-to-face restacking of graphene sheets. Graphene has a strong tendency to aggregate due to the •-• stacking perpendicular to the sheets, this lowers the specific surface area.

b. Surface chemical states. Graphene, especially those derived from graphite oxide, usually contains oxygen-containing functionalities. The functionalities on one hand bring some pseudo-capacitance beside electrical double layer capacitance. However, on the other hand, such impurities lower the electronic conductivity of graphene in magnitude order.

c. Defects of graphene sheets. Defects will affect the electron mobility of graphene remarkably thus influence its power performance.

d. Sheet size of graphene. It is known that the edge of graphene sheets shows higher specific capacitance than the basal plane. Thus graphene with smaller sheets is expected to show higher specific capacitance than those with larger sheets. On the other hand, with smaller sheets, there should be higher contact resistance between the sheets.

1.4 Objective of this thesis

This thesis focuses on the application of graphene material on electrochemical capacitors, aiming mainly to elucidate features that will improve the specific capacitance of reduced graphite oxide nanosheets.

Although a number of methods have been conducted aiming to separate graphene sheets in order to suppress restacking, and the fundamental capacitive behavior of mono- or few-layers of graphene is still far from clear. In Chapter 2, in order to obtain knowledge of the fundamental capacitive behavior of chemically-derived graphene in a monolayer state, a Layer-by-Layer approach was employed to produce reduced graphene oxide nanosheets with 1-10 monolayers spaced by polymer chains, and their electrochemical performance was studied in detail.

The edge-effect of graphene on its specific capacitance was reportd previously,[17] in order to get deeper knowledge on the root cause of the edge-effect, in Chapter 3, I tried to investigate the relationship of increasing on specific capacitance and the lateral size quantitatively. The lateral size of graphene was adjusted by using various ultrasonic treatments and evaluated using atomic force microscopy, and the electrochemical performance as well as their basic material characteristics was studied.

References

1. B. E. Conway, *Electrochemical Supercapacitors: Scientific Fundamentals and Technological Applications*, Kluwer Academic/Plenum Publishers, NY (1999).

2. R. K•tz and M. Carlen, Principles and applications of electrochemical capacitors, *Electrochimica Acta,* **45** (2000), 2483.

3. P. Sharma and T. S. Bhatti, A review on electrochemical double-layer capacitors, *Energ. Convers. Manage.* **51** (2010), 2901.

4. M. Jayalakshmi and K. Balasubramanian, Simple Capacitors to Supercapacitors – An Overview, *Int. J. Electrochem. Sci.,* **3** (2008), 1196.

5. J. W. Long, Electrochemical Capacitors Empowering the 21st Century, *Electrochem. Soc. Interface*, Spring 2008, 33.

6. J. R. Miller and A. F. Burke, Electrochemical Capacitors: Challenges and Opportunities for Real-World Applications, *Electrochem. Soc. Interface*, Spring 2008, 53.

7. H. E. Becker, U. S. Patent 2800616 (to General Electric) (1957).

8. R. A. Rightmire, U. S. Patent 3288641 (to The Standard Oil, SOHIO) (1966).

9. D. I. Boos, U. S. Patent 3536963 (to The Standard Oil, SOHIO) (1970).

10. B. E. Conway, J. O'M. Bockris and I. A. Ammar, The dielectric constant of the solution in the diffuse and Helmholtz double layers at a charged interface in aqueous solution, *Trans. Faraday Soc.* **47** (1951), 756.

11. J. Huang, B. G. Sumpter, and V. Meunier, A universal model for nanoporous carbon

supercapacitors applicable to diverse pore regimes, carbons, and electrolytes, *Chem. Eur. J.* **14** (2008), 6614.

12. P. Simon and Y. Gogotsi, Materials for electrochemical capacitors, *Nat. Mater.*, **7** (2008), 845.

13. C. Largeot, C. Portet, J. Chmiola, P. L. Taberna, Y. Gogotsi, and P. Simon, Relation between the ion size and pore size for an electric double-layer capacitor, *J. Am. Chem. Soc.,* **130** (2008), 2730

14. D. Hulicova, J. Yamashita, Y. Soneda, H. Hatori, and M. Kodama, Supercapacitors prepared from melamine-based carbon, *Chem. Mater.,* **17** (2005), 1241.

15. D. Hulicova, M. Kodama, and H. Hatori, Electrochemical performance of nitrogen-enriched carbons in aqueous and non-aqueous supercapacitors, *Chem. Mater.,* **18** (2006), 2318.

16. E. R. Pinero, K. Kierzek, J. Machnikowski, and F. Béguin, Relationship between the nanoporous texture of activated carbons and their capacitance properties in different electrolytes, *Carbon*, **44** (2006), 2498.

17. C. Zhang, D. Long, B. Xing, W. Qiao, R. Zhang, L. Zhan, X. Liang, and L. Ling, The superior electrochemical performance of oxygen-rich activated carbons prepared from bituminous coal, *Electrochem. Commun.*, **10** (2008), 1809.

18. K. Kierzek, E. Frackowiak, G. Lota, G. Gryglewicz, and J. Machnikowski, *Electrochimica Acta*, **49** (2004), 515.

19. E. Frackowiak and F. Beguin, Carbon materials for the electrochemical storage of

energy in capacitors, *Carbon*, **39** (2001), 937.

20. J. Lee, S. Yoon, T. Hyeon, S. M. Oh, and K. B. Kim, Synthesis of a new mesoporous carbon and its application to electrochemical double-layer capacitors, *Chem. Commun.*, **9** (1999), 2177.

21. W. Xing, S. Z. Qiao, R. G. Ding, F. Li, G. Q. Lu, Z. F. Yan, and H. M. Cheng, Superior electrical double layer capacitors using ordered mesoporous carbons, *Carbon*, **44** (2006), 216.

22. D Qu, Studies of the activated carbons used in double-layer supercapacitors, *J. Power Sources*, **109** (2002), 403.

23. K. Xia, Q. Gao, J. Jiang, and J. Hu, Hierarchical porous carbons with controlled micropores and mesopores for supercapacitor electrode materials, *Carbon*, **46** (2008), 1718.

24. W. Xing, C. C. Huang, S. P. Zhuo, X. Yuan, G. Q. Wang, D. Hulicova, Z. F. Yan, and G. Q. Lu, Hierarchical porous carbons with high performance for supercapacitor electrodes, *Carbon,* **47** (2009), 1715.

25. C. V. Guterl, E. Frackowiak, K. Jurewicz, M. Friebe, J. Parmentier, and F. Beguin, Electrochemical energy storage in ordered porous carbon materials, *Carbon*, **43** (2005), 1293.

26. J. A. Fernandez, S. Tennison, O. Kozynchenko, F. Rubiera, F. Stoeckli, and T. A. Centeno, Effect of mesoporosity on specific capacitance of carbons, *Carbon,* **47** (2009), 1598.

27. A. M. Polaczyk, C. M. Ghimbeu, C. V. Guterl, and E. Frackowiak, Carbon/MnO$_2$ composites for supercapacitor electrodes, *J. Solid State Chem.*, **183** (2010), 969.

28. D. Qu and H. Shi, Studies of activated carbons used in double-layer capacitors, *J. Power Sources*, **74** (1998), 99

29. A. G. Pandolfo and A. F. Hollenkamp, Carbon properties and their roll in supercapacitors, *J. Power Sources*, **157** (2006), 11.

30. H. Pan, J. Li, Y. Feng, Carbon nanotubes for supercapacitor, *Nanoscale Res. Lett.* **5** (2010), 654.

31. C. Emmenegger, P. Mauron, P. Sudan, P. Wenger, V. Hermann, R. Gallay, and A. Zuttel, Investigation of electrochemical double-layer capacitors electrodes based on carbon nanotubes and activated carbon materials, *J. Power Sources*, **124** (2003), 321.

32. T. Liu, U. S. Patent 7061749 B2 (2006).

33. J. Schindall, U. S. Patent 0258192 A1 (2007).

34. D. N. Futaba, K. Hata, T. Yamada, T. Hiraoka, Y. Hayamizu, Y. Kakudate, O. Tanaike, H. Hatori, M. Yumura, and S. Iijima, Shape-engineerable and highly densely packed single-walled carbon nanotubes and their application as super-capacitor electrodes, *Nat. Mater.*, **5** (2006), 987.

35. E. Bae, N. D. Kim, B. K. Kwak, J. Park, J. Lee, Y. Kim, K. Choi, and J. Yi, The effects of fullerene crystal structure on its electrochemical capacitance, *Carbon*, **48** (2010), 3676.

36. D. Wei, M. Scherer, C. Bower, P. Andrew, T. Ryhanen, and U. Steiner, A

nanostructured electrochromic supercapacitor, *Nano Lett.*, **12** (2012), 1857

37. W. Sugimoto, H. Iwata, Y. Yasunaga, Y. Murakami, and Y. Takasu, *Angew. Chem. Int. Ed.* **42** (2003), 4092.

38. W. Sugimoto, H. Iwata, Y. Murakami, and Y. Takasu, Electrochemical Capacitor Behavior of Layered Ruthenic Acid Hydrate, *J. Electrochem. Soc.*, **151** (2004), A1181.

39. W. Sugimoto, H. Iwata, K. Yokoshima, Y. Murakami, and Y. Takasu, Proton and electron conductivity in hydrous ruthenium oxides evaluated by electrochemical impedance spectroscopy: the origin of large capacitance, *J. Phys. Chem. B,* **109** (2005), 7330.

40. H. Li, R. Wang, and R. Cao, Physical and electrochemical characterization of hydrous ruthenium oxide/ordered mesoporous carbon composites as supercapacitor, *Microporous Mesoporous Mater.*, **111** (2008), 32

41. V. D. Patake and C. D. Lokhande, Chemical synthesis of nano-porous ruthenium oxide (RuO_2) film for supercapacitor application, *Appl. Surf. Sci.*, **254** (2008), 2820

42. M. S. Wu and P. C. Julia Chiang, Fabrication of nanostructured manganese oxide electrodes for electrochemical capacitors, *Electrochem. Solid-State Lett.*, **7** (2004), A123.

43. J. Jiang and A. Kucernak, Electrochemical supercapacitor material based on manganese oxide: preparation and characterization, *Electrochimica Acta*, **47** (2002), 2381.

44. S. W. Zhang and G. Z. Chen, Manganese oxide based materials for supercapacitors,

Energy Mater., **3** (2008), 186.

45. M. Jayalakshmi and K. Balasubramanian, Solution Combustion Synthesis of Fe_2O_3/C, Fe_2O_3-SnO_2/C, Fe_2O_3-ZnO/C Composites and their Electrochemical Characterization in Non-Aqueous Electrolyte for Supercapacitor Application, *Int. J. Electrochem. Sci.*, **4** (2009), 878.

46. G. A. Snook, P. Kao, and A. S. Best, Conducting-polymer-based supercapacitor devices and electrodes, *J. Power Sources*, **196** (2011), 1.

47. S. R. Sivakkumar and R. Saraswathi, Performance evaluation of poly(*N*-methylaniline) and polyisothianaphthene in charge-storage devices, *J. Power Sources*, **137** (2004), 322.

48. G. A. Snook, G. Z. Chen, D. J. Fray, M. Hughes, and M. Shaffer, *J. Electroanal. Chem.*, **568** (2004), 135.

49. K. S. Novoselov, A. K. Geim, S. V. Morozov, D. Jiang, Y. Zhang, S. V. Dubonos, I. V. Grigorieva, A. A. Firsov, Electric field effect in atomically thin carbon films, *Science*, **306** (2004), 666.

50. K. S. Novoselov, D. Jiang, F. Schedin, T. J. Booth, V. V. Khotkevich, S. V. Morozov, and A. K. Geim, Two-dimensional atomic crystals, *PNAS*, **102** (2005), 10451.

51. A. K. Geim and K. S. Novoselov, The rise of graphene, *Nat. Mater.*, **6** (2007), 183.

52. K. S. Novoselov, A. K. Geim, S. V. Morozov, D. Jiang, M. I. Katsnelson, I. V. Grigorieva, S. V. Dubonos, and A. A. Firsov, Two-dimensional gas of massless Dirac fermions in graphene, *Nature*, **438** (2005), 197.

53. Y. Zhang, J. W. Tan, H. L. Stormer, and P. Kim, Experimental observation of the quantum Hall effect and Berry's phase in graphene. *Nature*, **438** (2005), 201.

54. J. C. Meyer, A. K. Geim, M. I. Katsnelson, K. S. Novoselov, T. J. Booth, and S. Roth, The structure of suspended graphene sheets, *Nature*, **446** (2007), 60.

55. K. I. Bolotin, K. J. Sikes, Z. Jiang, M. Klima, G. Gudenberg, J. Hone, P. Kim, and H. L. Stormer, Ultrahigh electron mobility in suspended graphene, *Solid State Commun.*, **146** (2008), 351.

56. A. A. Balandin, S. Ghosh, W. Bao, I. Calizo, D. Teweldebrhan, F. Miao, and C. N. Lau, Superior thermal conductivity of single-layer graphene, *Nano Lett.*, **8** (2008), 902.

57. Novoselov, K. S.; Geim, A. K.; Morozov, S. V.; Jiang, D.; Zhang, Y.; Dubonos, S. V.; Grigorieva, I. V.; Firsov, A. A. Electric Field Effect in Atomically Thin Carbon Films. *Science* **306** (2004), 666.

58. W. Liu, H. Li, C. Xu, Y. Khatami, and K. Banerjee, Synthesis of high-quality monolayer and bilayer graphene on copper using chemical vapor deposition, *Carbon* **49** (2011), 4122.

59. S. Bae, H. Kim, Y. Lee, X. Xu, J. S. Park, et al., Roll-to-roll production of 30-inch graphene films for transparent electrodes, *Nat. Nanotech.*, **5** (2010), 574.

60. H. An, W. Lee, and J. Jung, Graphene synthesis on Fe foil using Thermal CVD, *Current Appl. Phys.* **11** (2011), S81.

61. Z. Y. Juang, C. Y. Wu, C. W. Lo, W. Y. Chen, C. F. Huang, J. C. Hwang, F. R. Chen, K. C. Leou and C. H. Tsai, Synthesis of graphene on silicon carbide substrates at low

temperature, *Carbon*, **47** (2009), 2026.

62. S. Pei, H. M. Cheng, The reduction of graphene oxide, *Carbon,* **50** (2012), 3210.

63. X. Li, C. W. Magnuson, A. Venugopal, J. An, J. W. Suk, B. Han, M. Borysiak, W. Cai, A. Velamakanni, Y. Zhu, L. Fu, E. M. Vogel, E. Voelkl, L. Colombo, and R. S. Ruoff, Graphene films with large domain size by a two-step chemical vapor deposition process, *Nano Lett.* **10** (2010), 4328.

64. T. Szabo, A. Szeri, and I. Dekany, Composite graphitic nanolayers prepared by self-assembly between finely dispersed graphite oxide and a cationic polymer, *Carbon* **43** (2005), 87.

65. S. Gilje, S. Han, M. Wang, K. Wang, and R. Kaner, A Chemical Route to Graphene for Device Applications, *Nano Lett.* **7** (2007), 3394.

66. S. Park and R. S. Ruoff, Chemical methods for the production of graphenes, *Nat. Nanotech.* **4** (2009), 217.

67. S. Park, J. An, J. R. Potts, A. Velamakanni, S. Murali, and R. S. Ruoff, Hydrazine-reduction of graphite- and graphene oxide, *Carbon*, **49** (2011), 3019.

68. J. Xia, F. Chen, J. Li, and N. Tao, Measurement of the quantum capacitance of graphene, *Nat. Nanotech.*, **4** (2009), 505.

69. S. Vivekchand, C. S. Rout, K. S. Subrahmanyam, A. Govindaraj, and C. Rao, Graphene-based electrochemical supercapacitors, *J. Chem. Sci.*, **120** (2008), 9.

70. M. D. Stoller, S. Park, Y. Zhu, J. An, and R. S. Ruoff, Graphene-Based Ultracapacitors, *Nano Lett.* **8** (2008), 3498.

71. Y. Wang, Z. Shi, Y. Huang, Y. Ma, C. Wang, M. Chen, and Y. Chen, Supercapacitor Devices Based on Graphene Materials, *J. Phys. Chem. C*, **113** (2009), 13103.

72. W. Lv, D. M. Tang, Y. B. He, C. H. You, Z. Q. Shi, et al., Low-Temperature Exfoliated Graphenes: Vacuum-Promoted Exfoliation and Electrochemical Energy Storage, *ACS Nano*, **3** (2009), 3730.

73. Y. Zhu, S. Murali, M. D. Stoller, A. Velamakanni, R. D. Piner, and R. S. Ruoff, Microwave assisted exfoliation and reduction of graphite oxide for ultracapacitors, *Carbon*, **48** (2010), 2106.

74. Y. Zhu, M. D. Stoller, W. Cai, A. Velamakanni, R. D. Piner, D. Chen, and R. S. Ruoff, Exfoliation of graphite oxide in propylene carbonate and thermal reduction of the resulting graphene oxide platelets, *ACS Nano*, **4** (2010), 1227.

75. Q. Wu, Y. Xu, Z. Yao, A. Liu, and G. Shi, Supercapacitors based on flexible graphene/polyaniline nanofiber composite films, *ACS Nano*, **4** (2010), 1963.

76. C. Liu, Z. Yu, D. Neff, A. Zhamu, and B. Z. Jang, Graphene-Based Supercapacitor with an Ultrahigh Energy Density, *Nano Lett.* **10** (2010), 4863.

77. S. Chen, J. Zhu, X. Wu, Q. Han, and X. Wang, Graphene oxide-MnO_2 nanocomposites for supercapacitors, *ACS Nano*, **4** (2010), 2822.

78. J. Yan, T. Wei, B. Shao, F. Ma, Z. Fan, M. Zhang, C. Zheng, Y. Shang, W. Qian, and F. Wei, Electrochemical properties of graphene nanosheet-carbon black composites as electrodes for supercapacitors, *Carbon*, **48** (2010), 1731.

79. J. R. Miller, R. A. Outlaw, and B. C. Holloway, Graphene Double-Layer Capacitor

with ac Line-Filtering Performance, *Science,* **329** (2010), 1637.

80. L. Zhang and G. Shi, Preparation of Highly Conductive Graphene Hydrogels for Fabricating Supercapacitors with High Rate Capability, *J. Phys. Chem. C*, **115** (2011), 17206.

81. Q. Cheng, J. Tang, J. Ma, H. Zhang, N. Shinya and L. C. Qin, Graphene and nanostructured MnO_2 composite electrodes for supercapacitors, *Carbon*, **49** (2011), 2917.

82. Y. Zhu, S. Murali, M. D. Stoller, et al., Carbon-Based Supercapacitors Produced by Activation of Graphene, *Science*, **332** (2011), 1537.

83. M. F. El-Kady, V. Strong, S. Dubin, R. B. Kaner, Laser Scribing of High-Performance and Flexible Graphene-Based Electrochemical Capacitors, *Science*, **335** (2012), 1326.

84. J. Han, L. L. Zhang, S. Lee, J. Oh, K. S. Lee, J. R. Potts, J. Ji, X. Zhao, R. S. Ruoff, and S. Park, Generation of B-Doped Graphene Nanoplatelets Using a Solution Process and Their Supercapacitor Applications, *ACS Nano*, **7** (2013), 19.

85. Z. Lei, T. Sakai, W. Sugimoto, Lateral Size Effect on Electrochemical Capacitor Performance of Reduced Graphite Oxide Nanosheets. *Electrochem.* **80** (2013), 873.

86. A. K. Sarker and J. D. Hong, Layer-by-Layer Self-Assembled Multilayer Films Composed of Grpahene/Polyaniline Bilayers: High-Energy Electrode Materials for Supercapacitors, *Langmuir* **28** (2012), 12637.

87. G. Williams, B. Seger, and P. V. Kamat, TiO_2-Graphene Nanocomposites.

UV-Assisted Photocatalytic Reduction of Graphene Oxide. *ACS Nano* **2** (2008), 1487.

88. G. K. Dimitrakakis, E. Tylianakis, and G. E. Froudakis, Pillared Graphene: A New 3-D Network Nanostructure for Enhenced Hydrogen Storage. *Nano Lett.* **8** (2008), 3166.

89. A. K. Mishra and S. Ramaprabhu, Functionalized Graphene-Based Nanocomposites for Supercapacitor Application. *J. Phys. Chem. C* **115** (2011), 14006.

90. S. Yin, Y. Zhang, J. Kong, C. Zou, C. Li, X. Lu, F.Y. C. Boey, and X. Chen, Assembly of graphene sheets into hierarchical structure for high-performance energy storage. *ACS Nano*, **5** (2011), 3831.

91. Z. Xu, Z. Li, C. Holt, X. Tan, H. Wang, B. S. Amirkhiz, T. Stephenson, and D. Mitlin, Electrochemical Supercapacitor Electrodes from Sponge-like Graphene Nanoarchitectures with Ultrahigh Power Density. *J. Phys. Chem. Lett.* **3** (2012), 2928.

92. M. F. El-Kady and R. B. Kaner, Scalable fabrication of high-power graphene micro-supercapacitors for flexible and on-chip energy storage. *Nat. Communi.*, DOI: 10.1038/ncomms2446 (2013), 1.

Chapter 2

Achieving 100% Utilization of Reduced Graphene Oxide by Layer-by-Layer Assembly: Insight into the capacitance of a monolayer of graphene
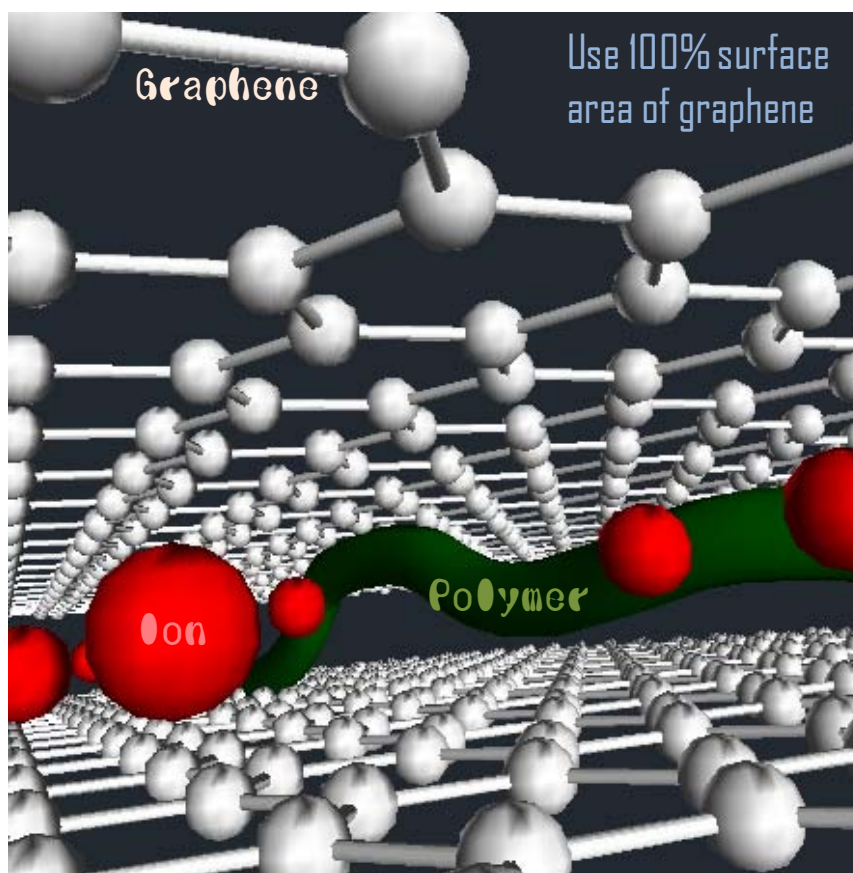
2.1 INTRODUCTION

Graphene has recently attracted much interests as a promising electrode material for electrochemical capacitors owing to its theoretically high specific surface area and good electronic conductivity.[1-7] A number of studies have been reported for the fabrication of electrochemical capacitors using graphene-based materials as the electrode.[8-13] However, the achieved capacitance of these studies are still far from the maximum value of ~550 F g^{-1} calculated based on the theoretical surface area of 2630 m^2 g^{-1} and the commonly accepted value of ~21 μF cm^{-2} for electrical double layer capacitance.[14] Naturally, one of the reasons that the theoretical capacitance cannot be achieved is that the surface area of graphene-based electrodes is smaller than its theoretical value due to restacking. In addition, the capacitive performance of graphene-based materials is known to be affected by a number of factors, such as the degree of exfoliation (number of graphene layers),[15, 16] lateral size of individual sheets,[17, 18] defects,[2, 19] degree of oxidation,[20] and so on.[21] Such factors have inhibited characterization of the intrinsic properties of these materials. A simplified model electrode study with well-defined, countable graphene layers should contribute to the understanding of the maximum capacitance that can be obtained when ~100% utilization of the surface is achieved.

We chose to adopt the electrostatic layer-by-layer (LbL) self-assembly technique, a widely used approach for fabrication of well-defined and controlled thin films.[22] By alternately depositing positively and negatively charged nano-materials, one can readily fabricate multi-component materials in a controllable manner. As LbL affords

well-defined thin films of manipulable and countable alternating layers of graphene oxide, we anticipated that the LbL self-assembly approach to fabricate mono-layered to multi-layered graphene oxide thin films would serve as an ideal model system to achieve a spaced nano-architecture of graphene electrodes for charge storage applications. LbL self-assembly has been utilized by several groups for fabrication of thin films consisting of graphene oxide or similar materials.[23-29] These studies have proven that combining graphene with other electrode materials such as carbon nanotubes, conducting polymers and metal oxides results in enhanced capacitive performance. Unfortunately, graphene is used merely as a conducting agent or a conductive support in these composites, not differing much from other traditional carbonaceous materials. To the best of our knowledge, none of these studies have succeeded in characterizing the fundamental electrochemical capacitive behavior of mono-layer graphene.

Here, we report the fabrication of thin films composed of mono-layered reduced graphene oxide suitable for characterizing the capacitance of a single layer of graphene. The LbL technique was employed to fabricate thin films composed of alternating layers of mono-layered graphene oxide (GO) and a polycation, followed by reduction of GO to obtain reduced graphene oxide (rGO). The polycation is anticipated to act as a polymeric binder preventing individual rGO from restacking and allow penetration of electrolyte, thus making full use of its surface for application as electrodes for electrochemical capacitors. A series of thin films with 1 to 10 mono-layers of rGO were

investigated in detail using cyclic voltammetry and electrochemical impedance spectroscopy in acidic and neutral electrolyte in order to elucidate the fundamental capacitive behavior of the multi-layered rGO electrodes.

2.2 EXPERIMENTAL

Graphite oxide was prepared by oxidization of graphite powder (Z-5F, ITO GRAPHITE Co., Ltd.), following the Hummers method.[30] Briefly, graphite powder was mixed with $NaNO_3$ and added into concentrated H_2SO_4. $KMnO_4$ was added slowly into the slurry with stirring (cooled in ice-water) and then aged for 4 days at room temperature. After the completion of the oxidization of graphite, water was added to the brownish slurry, filtered and washed thoroughly with diluted HCl and methanol in sequence. The obtained brown powder (graphite oxide) was dried overnight and ground to powder state. Graphite oxide (20 mg) was dispersed in 20 mL of ultrapure water (> 18 M• cm) and exfoliated with assistance of mild ultrasonic treatment. Colloidal mono-layer graphene oxide was obtained after removal of non-exfoliated graphite oxide via centrifugation (2000 rpm for 30 min).

Poly(diallyldimethylammonium chloride) (PDDA, 20 wt% aqueous solution, Aldrich) was used as the counter polycation to electrostatically deposit GO layer-by-layer. The LbL deposition was conducted with a DC 4200 dip-coating system (AIDEN CO., Ltd.). Briefly, the substrate (Au plate, quartz glass or silicon wafer) was dipped in a diluted PDDA solution (2 wt%) for 10 min, washed carefully with ultrapure water and dried in

air, then dipped in colloidal GO (diluted to 0.2 g L^{-1}) for 20 min, washed again with ultrapure water and dried in air. One cycle of this procedure gives a film composed of a mono-layer graphene oxide, $(PDDA/GO)_1$, and repetitive cycles affords multi-layered graphene oxide films, $(PDDA/GO)_n$ with n=2-10.

The deposited films were reduced either by gas-phase or chemical reduction. Gas-phase reduction was conducted by thermal treatment at 200 °C under H_2/N_2=1/9 flow for 2 h. Chemical reduction was conducted by dipping $(PDDA/GO)_n$ films in an aqueous solution of 0.1 M N_2H_4 (Wako Pure Chemical) for 24 h at 60 °C, followed by washing with ultrapure water. The H_2- and N_2H_4-reduced samples will be denoted $(PDDA/rGO)_n$-H_2 and $(PDDA/ rGO)_n$-N_2H_4, respectively.

The surface morphology of $(PDDA/GO)_1$ deposited on Si wafer was observed with atomic force microscopy (AFM, SPM-400, Seiko Instruments Inc.). UV-vis spectroscopy (U-4100, Hitachi High-Technologies Corp.) was employed for characterization of the amount of GO deposited on quartz glass by each deposition cycle. X-ray photoelectron spectrometry (XPS, AXIS-ULTRA DLD, Kratos Analytic Ltd.) was conducted for chemical analysis of powder samples of rGO synthesized by drying colloidal GO at 60 °C, and reduced accordingly.

Cyclic voltammetry (HZ-5000, Hokuto Denko Corp.) was carried out with a three-electrode beaker cell, in which the working electrode was $(PDDA/rGO)_n$ (n=1-10) deposited on one side of a flat gold substrate of 1×1 cm with the back side masked. An Ag/AgCl (sat. KCl) electrode was used as the reference electrode, and a Pt mesh was

employed as the counter electrode. 0.5 M H_2SO_4 or Na_2SO_4 was used as the electrolyte.

Potential scans were conducted between 0.2-1.2 V vs. RHE at 500, 200, 50, 20, 5 and 2

mV s^{-1} after 500 break-in cycles at 50 mV s^{-1}. Electrochemical impedance spectroscopy

(1287 Electrochemical Interface, 1255B Frequency Response Analyzer, Solartron) was

carried out after cyclic voltammetry. A Pt wire was used as the reference electrode in

order to minimize IR loss at high frequency. Impedance measurements were conducted

at 0.2, 0.4, 0.6, 0.8, 1.0 and 1.2 V vs. RHE by sweeping the frequency from 100 kHz to

10 mHz with an amplitude of 5 mV.

2.3 RESULTS AND DISCUSSION

AFM images of $(PDDA/GO)_1$ (Fig. 2-1) revealed GO with lateral size of

sub-micrometers to several micrometers. The thickness of individual GO was ~1 nm,

indicating successful exfoliation, with negligible amount of non-exfoliated graphite

oxide or few-layer sheets. Under the film processing conditions applied, over 90% of

the substrate was covered by GO, with some overlapping or folding of GO. The

uniformity of $(PDDA/GO)_n$ (n = 1-10) films was probed by UV-vis spectroscopy. The

absorbance increases proportionally as the number of (PDDA/GO) layers increases (Fig.

2-2), indicating that the same amount of GO was deposited per deposition cycle.

Figure 2-3 shows the cyclic voltammograms of $(PDDA/rGO)_n$ (n=1, 2, 3, 5, 10)

reduced by H_2 or N_2H_4 in H_2SO_4 at 20 mV s^{-1}. The specific capacitance is plotted in

Figure 2-4 as a function of the number of layers. Both series exhibited a linear increase

in specific capacitance as the number of layers increased, indicating an equal charge storage contributed by each rGO layer. This observation strongly suggests that all of the rGO spaced by PDDA are utilized for charge storage. From the slope of Figure 2-4, an average specific capacitance of 115 and 75 $\mu F \ cm^{-2}$ per layer of rGO is derived for $(PDDA/rGO)_n$-H_2 and $(PDDA/rGO)_n$- N_2H_4, respectively.

As redox peaks at ~0.6 V were observed for both series in H_2SO_4, the 10-layer samples reduced by both methods were also evaluated in 0.5 M Na_2SO_4 in order to exclude the influence from the surface redox reaction (pseudocapacitance). No redox peaks were observed in neutral electrolyte (Figure 2-5), thus allowing characterization of the electrical double layer capacitance (C_{dl}). The C_{dl} values were 66 and 52 μF per rGO layer in Na_2SO_4 for $(PDDA/rGO)_{10}$-H_2 and $(PDDA/rGO)_{10}$-N_2H_4, respectively. The pseudo-capacitance related to surface redox reaction (C_{red}), which can be obtained from the difference in specific capacitance in H_2SO_4 and Na_2SO_4, is calculated to be 49 and 23 μF per rGO layer for $(PDDA/rGO)_{10}$-H_2 and $(PDDA/rGO)_{10}$-N_2H_4 in H_2SO_4, respectively. Assuming that both sides of each rGO layer contribute equally to the capacitance, we obtain $C_{dl} = 33 \ \mu F \ cm^{-2}$, $C_{red} = 25 \ \mu F \ cm^{-2}$ for the H_2-reduced samples, and $C_{dl} = 26 \ \mu F \ cm^{-2}$ and $C_{red} = 12 \ \mu F \ cm^{-2}$ for N_2H_4-reduced samples in H_2SO_4.

In order to quantify the content of the surface functional groups in the samples, H_2- and N_2H_4-reduced rGO powders were prepared and evaluated with X-ray photoelectron spectroscopy (Figure 2-6). The oxygen content in H_2- and N_2H_4-reduced rGO was O/C=0.21 and 0.10, respectively. The doubled oxygen content of H_2-reduced sample

brings approximately doubled redox capacitance (C_{red}=25 μF cm^{-2} vs. 12 μF cm^{-2}) compared to the N$_2$H$_4$-reduced counterpart. Therefore, the C_{red} in acidic electrolyte can rationally be attributed to the oxygen-containing functional groups.

In order to gain information on the kinetics of the charge storage process, electrochemical impedance spectroscopy (EIS) and transmission line model (TLM) analysis was conducted.[31-33] Here we employ the EIS and TLM modeling for the characterization of (PDDA/rGO)$_n$ (n= 5, 10) reduced by H$_2$ or N$_2$H$_4$. The model structure is composed of layers of rGO with slit pores with lateral size the same as the gold substrate (1×1 cm) (Figure 2-7). The equivalent circuit inside the interlayer gaps can be expressed as Z_{TLM} (shown in Figure 2-8), which has a total impedance according to the de Levie model,[34]

$$Z_{TLM} = R_{TLM}^* \, Z^* \, \coth\left(\sqrt{\frac{R_{TLM}^*}{Z^*}}X\right)$$

$$Z^* = \frac{Z^{**}}{l}$$

$$Z^{**} = \frac{Z_R}{1+(j\omega)^{p_{II}}(Z_R)C_{TLM}}, \text{ where } Z_R = R_f + \frac{1}{j\omega C_{red}}$$

where X is the length of the slit pore along the ion penetration direction, Z^* is the impedance per unit length in the slit pores, Z^{**} is the impedance per unit area, l is the perimeter of cross-section of the slit pore, j is the imaginary unit and, $\bullet$ (=2$\bullet f$, where f is frequency) is the angular frequency.

Taking into account of the inductance (L) at high frequency, the electrolyte resistance (R_{sol}), and the capacitance and charge transfer resistance at outer surfaces (R_{ct}, C_s), an equivalent circuit for the impedance simulation of (PDDA/rGO)$_n$ was built up as shown in Figure 2-8. The impedance of Part I, II and III in Figure 2-8 are expressed as,

$$Z_I = j\omega L$$

$$Z_{II} = R_{sol}$$

$$Z_{III} = \frac{R_{ct}}{1 + (j\omega)^{p_1} R_{ct} C_s}$$

Thus the impedance for the whole circuit is:

$$Z = Z_I + Z_{II} + Z_{III} + Z_{TLM}$$

In the simulation, the length of the slit pore along the ion penetration direction for all samples is X=1 cm, equal to the geometric size of the electrode, and the perimeter of the slit pores is l =2 cm × n layers. Typical simulation results are shown in Figs. 2-9 - 2-14, showing excellent resemblance between raw data and simulated curves at low and high frequency.

Figure 2-15 shows C_{TLM} and R_{TLM}^{*} obtained from TLM-simulation of (PDDA/rGO)$_{10}$ reduced by both methods in Na_2SO_4. Note that in Na_2SO_4 the frequency response reflects the pure electric double-layer capacitive behavior. (PDDA/rGO)$_{10}$-H_2 shows a C_{TLM} of ~25 μF cm^{-2} at 0.2-1.0 V and ~10 μF cm^{-2} at 1.2 V. (PDDA/rGO)$_{10}$-N_2H_4 shows C_{TLM} of 12-20 μF cm^{-2} between 0.2-1.2 V. These values are in good agreement with that obtained from cyclic voltammetry. R_{TLM}^{*} shows higher

values for the N_2H_4-reduced (O/C=0.10) compared to the H_2-reduced counterpart (O/C=0.21). Since samples with lower O/C have lower ionic conductivity due to higher hydrophobicity and higher electronic conductivity, the R_{TLM}^* is suggested to be dominated by ionic conductivity. In other words, $(PDDA/rGO)_{10}$-H_2 with higher O/C and lower electronic conductivity has higher C_{TLM} and lower R_{TLM}^*. Thus, leaving a certain amount of surface functionalities seems to be advantageous for non-Faradaic electrical double layer charging.

C_{TLM} obtained from the simulation of $(PDDA/rGO)_n$-H_2 and -N_2H_4 in H_2SO_4 are shown in Figure 2-16 in comparison with that in Na_2SO_4. The 5- and 10-layered samples show similar C_{dl} in H_2SO_4 and Na_2SO_4. C_{red} obtained from the simulation of $(PDDA/rGO)_n$ (n = 5, 10) are shown in Figure 2-17. C_{red} shows a maximum at ~0.6 V for all samples, with higher values for the H_2-reduced ones due to the higher content of oxygen functionalities, in agreement with cyclic voltammetry data. R_{TLM}^* shows higher values in Na_2SO_4 compared to that in H_2SO_4 (Figure 2-18), which can be attributed to the lower ionic conductivity of the electrolyte in the slit pores. R_{TLM}^* has a tendency to increase with potential, which may be a sign of higher electronic resistance at higher potential. This may be the reason for the smaller C_{dl} values observed by both CV and EIS at high potential. In H_2SO_4, R_{TLM}^* for the H_2-reduced samples (O/C=0.21) shows slightly higher values compared to the N_2H_4-reduced counterparts (O/C=0.10), which is the opposite trend as that seen in Na_2SO_4. In H_2SO_4, as the ionic conductivity in the slit pores is sufficiently high the electronic resistance dominates the resistance in the pores,

(PDDA/rGO)$_{10}$-N$_2$H$_4$ with lower O/C and higher electronic conductivity has lower $R_{\text{TLM}}{}^*$. Combining the change of $R_{\text{TLM}}{}^*$ in both H$_2$SO$_4$ and Na$_2$SO$_4$, it is concluded that $R_{\text{TLM}}{}^*$ is influenced more by electronic conductivity of rGO in H$_2$SO$_4$ and more by ionic conductivity in Na$_2$SO$_4$.

Analysis of the cyclic voltammograms and impedance spectroscopy shows that the electrical double layer capacitance of rGO is roughly 20 μF cm^{-2}. The 10-layered film is ~11 nm thick based on the basal spacing of the lamellar structure. Then, the packing density is roughly 0.6 g cm^{-3} and the volumetric capacitance of 364 F cm^{-3}. This shows the potential of this type of nanoarchitecture for high volumetric density devices.

The C_{dl} value can also be translated into the specific capacitance of graphene per electrochemically active surface area. Since there is some overlapping of individual rGO layers, the capacitance values stated above assuming that the electrochemically active surface area is the same as number of layers times the footprint area should be slightly overestimated. Taking the coverage of 90% and a rough estimation of 50% overlapping of individual rGO layers in each layer, the specific capacitance per active surface area is estimated to be ~15 μF cm^{-2}, and the gravimetric capacitance is ~400 F g^{-1} from the theoretical surface area of 2,630 m^2 g^{-1}.

2.4 CONCLUSIONS

Lamellar nano-architectures composed of reduced graphene oxide spaced by poly(diallyldimethylammonium) were successfully fabricated using electrostatic

layer-by-layer self-assembly and reduction with H_2 or N_2H_4. The electrical double layer capacitance was evaluated with neutral Na_2SO_4, and pseudo-capacitance originating from oxygen functionalities in H_2SO_4 was analyzed accordingly. Pseudo-capacitance in H_2SO_4 increases proportionally with the increase in the oxygen functionality groups. Cyclic voltammetry and electrochemical impedance spectroscopy indicated a full utilization of rGO layers for charge storage could be obtained in the layer-by-layer assembled thin films. Transmission-line modeling has shown that the charge storage capability is affected by the electronic conductivity and the ionic conductivity in the system, which varies with the degree of reduction of the rGO and the type of electrolyte used. The capacitive behavior in the slit pores is influenced more by electronic conductivity of rGO when H_2SO_4 (a highly conductive electrolyte) is used and affected more by the ionic conductivity in Na_2SO_4 (a poorly conductive electrolyte). The electrical double layer capacitance per electrochemically active surface area of rGO is estimated to be roughly 15 μF cm^{-2} and gravimetric capacitance as ~400 F g^{-1}. It is suggested that graphene may be used as an electrode material with high volumetric capacitance by nanoarchitectural design of electrodes.

Figures
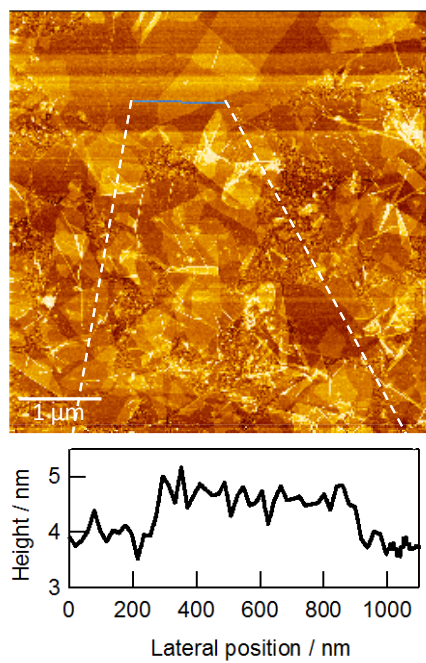
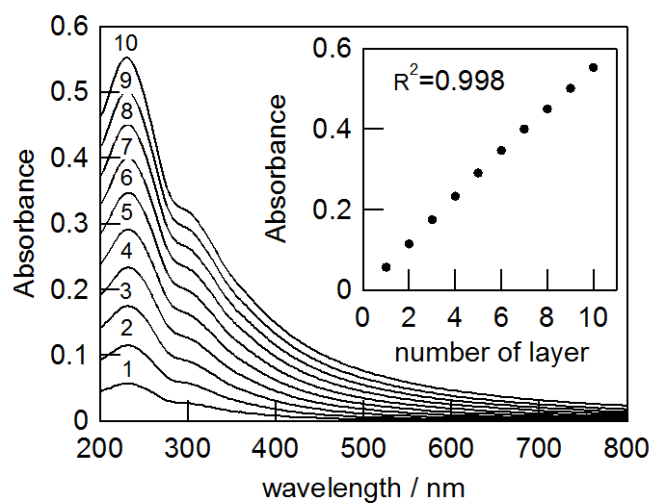Figure 2-1. A typical AFM image of (PDDA/GO)$_1$ deposited on silicon substrate.

Figure 2-2. UV-vis absorbance spectra of (PDDA/GO)$_n$ (n = 1-10). Inset: Absorbance of

(PDDA/GO)$_n$ (n = 1-10) at wavelength of 230 nm as a function of the number of
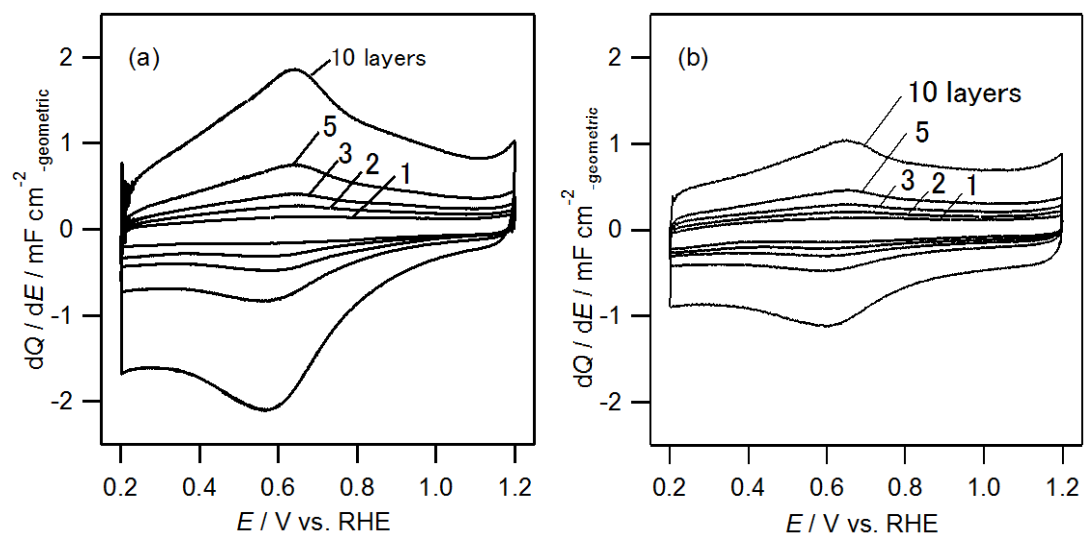
deposited layers.

Figure 2-3. Cyclic voltammograms of (PDDA/rGO)$_n$ (n=1, 2, 3, 5, 10) reduced by (a)

H$_2$ and (b) N$_2$H$_4$ in 0.5 M H$_2$SO$_4$ at 20 mV s^{-1}.
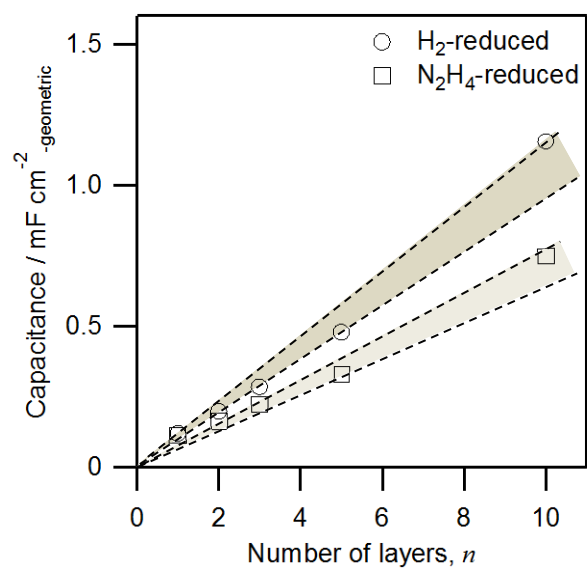
Figure 2-4. Specific capacitance (in 0.5 M H_2SO_4) of $(PDDA/rGO)_n$ as a function of number of layers n.
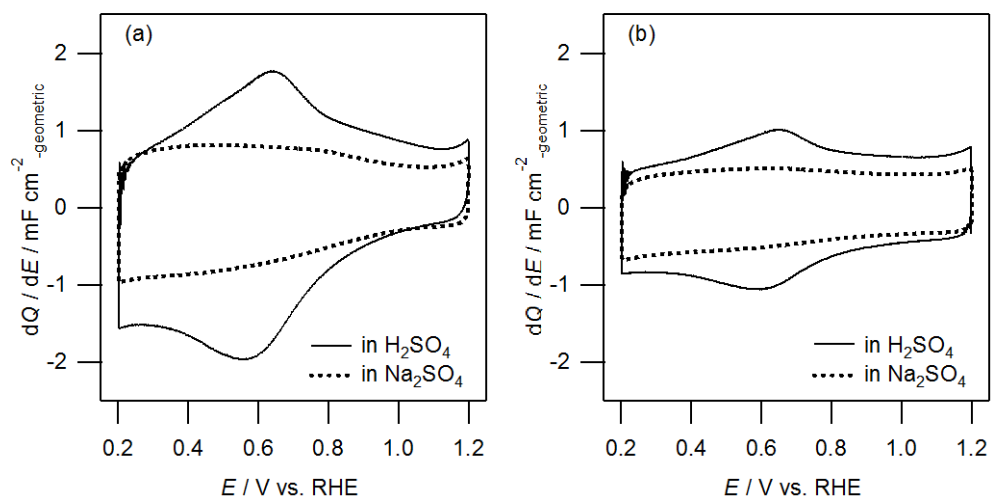
Figure 2-5. Cyclic voltammograms of (PDDA/rGO)$_{10}$ reduced by (a) H$_2$ and (b) N$_2$H$_4$

in 0.5 M H$_2$SO$_4$ or Na$_2$SO$_4$ at 20 mV s^{-1}.
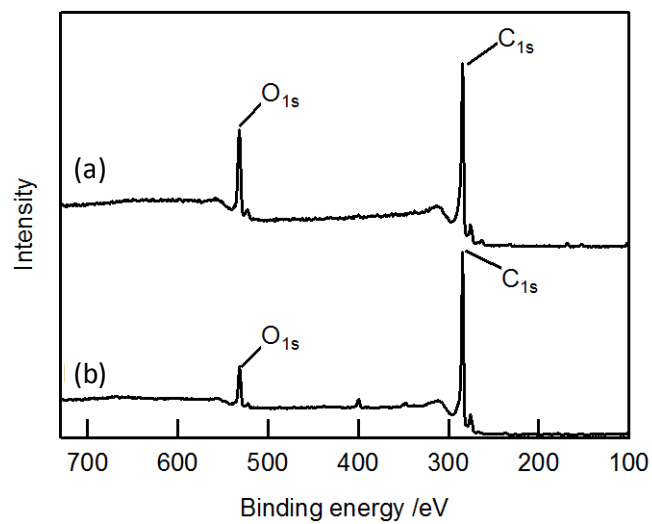
Figure 2-6. X-ray photoelectron spectra of (a) H_2- and (b) N_2H_4-reduced rGO powders. The O/C atomic ratio for H_2- and N_2H_4-reduced sample was 0.21 and 0.10, respectively.
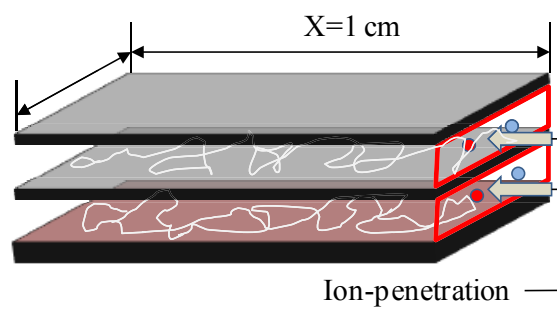
X=1 cm
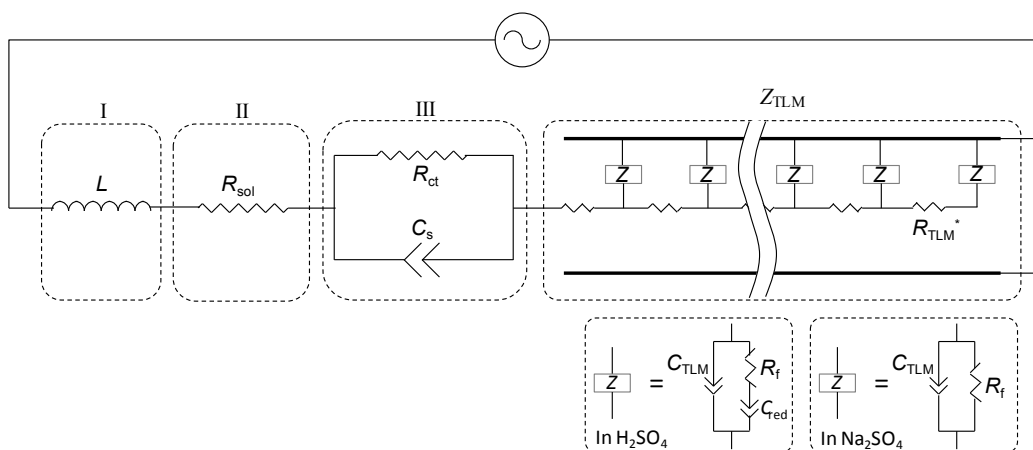
Ion-penetration

Figure 2-7. Model structure of (PDDA/rGO)$_n$.

Figure 2-8. Equivalent circuit for simulation of $(PDDA/rGO)_n$. Refer to text for definition of labels.
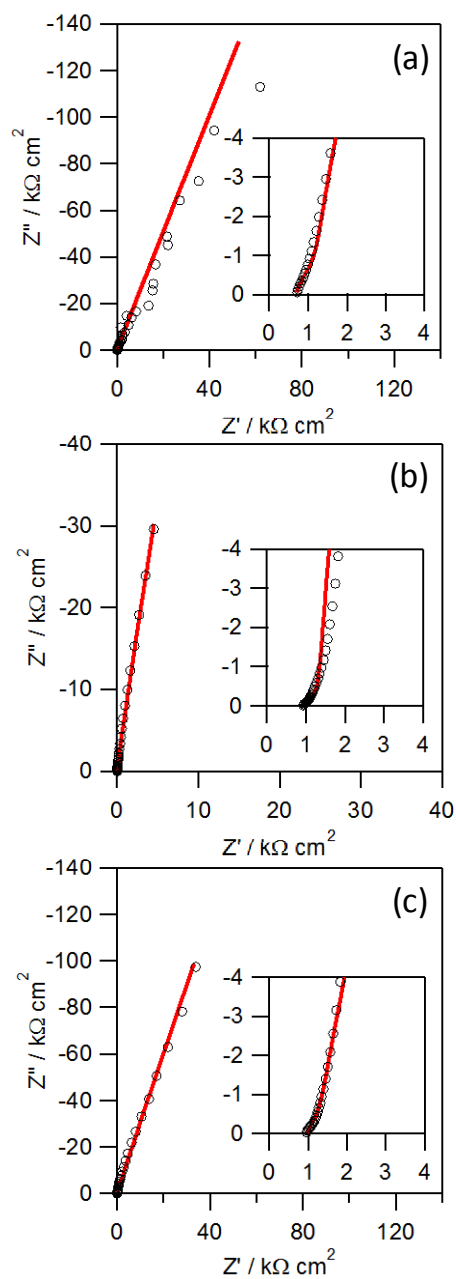
Figure 2-9. Experimental (open plots) and simulated (lines) results for

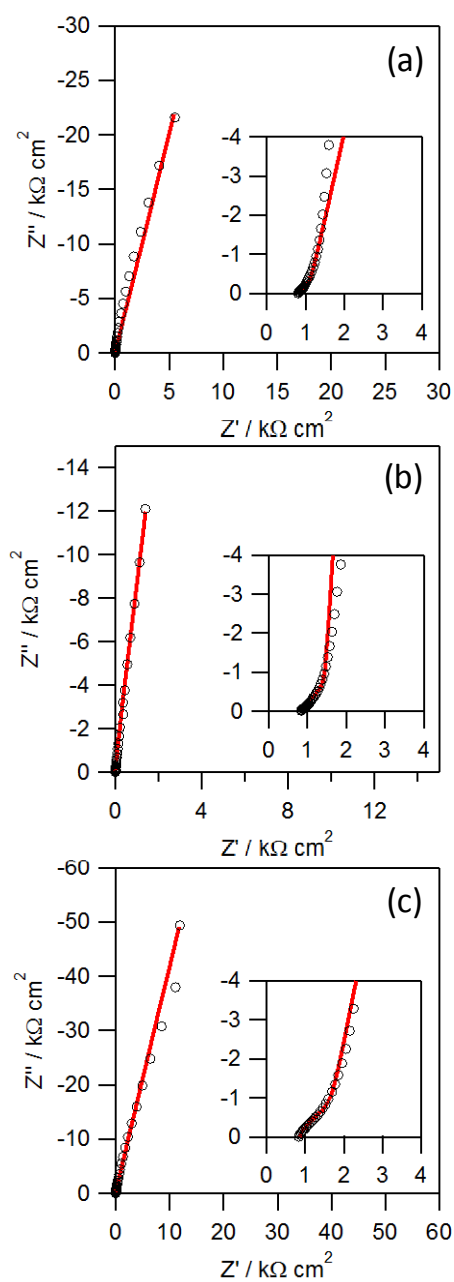$(PDDA/rGO)_5$-H_2 in H_2SO_4 at (a) 0.2 V, (b) 0.6 V, (c) 1.0 V vs. RHE.

Figure 2-10. Experimental (open plots) and simulated (lines) results for

(PDDA/rGO)$_{10}$-H$_2$ in H$_2$SO$_4$ at (a) 0.2 V, (b) 0.6 V, (c) 1.0 V vs. RHE.
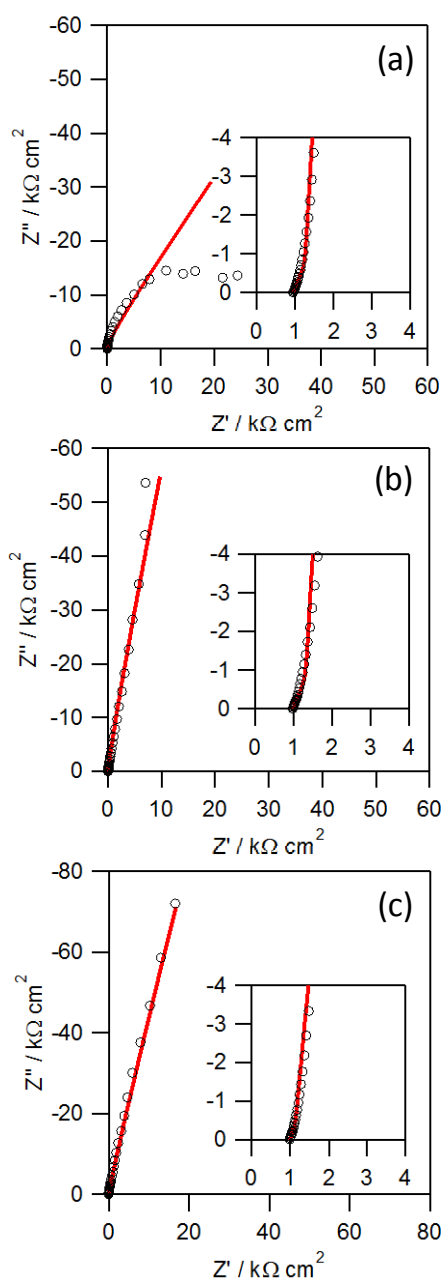
Figure 2-11. Experimental (open plots) and simulated (lines) results for

(PDDA/rGO)$_5$-N$_2$H$_4$ in H$_2$SO$_4$ at (a) 0.2 V, (b) 0.6 V, (c) 1.0 V vs. RHE.

Figure 2-12. Experimental (open plots) and simulated (lines) results for

(PDDA/rGO)$_{10}$-N$_2$H$_4$ in H$_2$SO$_4$ at (a) 0.2 V, (b) 0.6 V, (c) 1.0 V vs. RHE.

Figure 2-13. Experimental (open plots) and simulated (lines) results for

$(PDDA/rGO)_{10}$-H_2 in Na_2SO_4 at (a) 0.2 V, (b) 0.6 V, (c) 1.0 V vs. RHE.
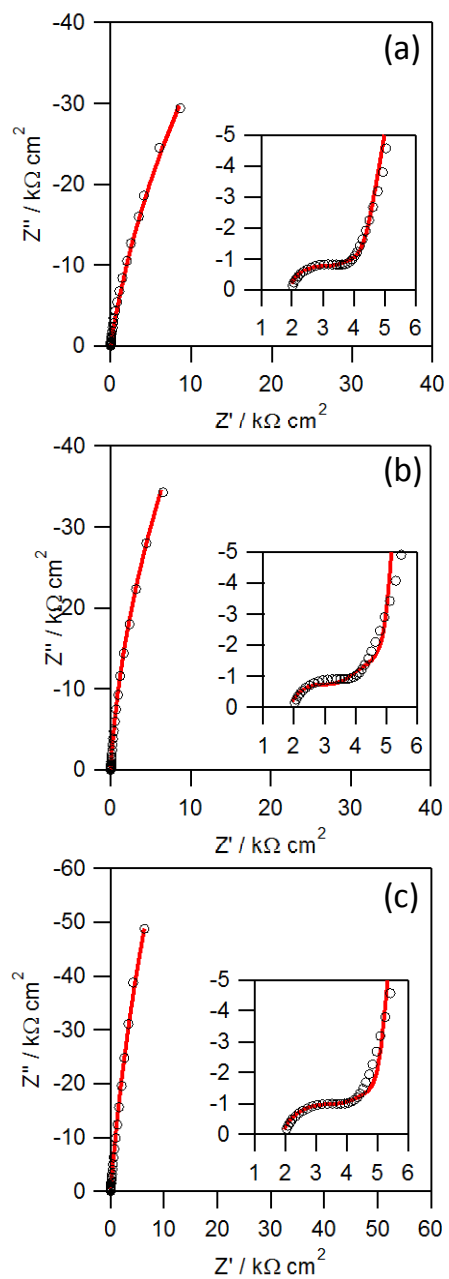
Figure 2-14. Experimental (open plots) and simulated (lines) results for

$(PDDA/rGO)_{10}$-N_2H_4 in Na_2SO_4 at (a) 0.2 V, (b) 0.6 V, (c) 1.0 V vs. RHE.
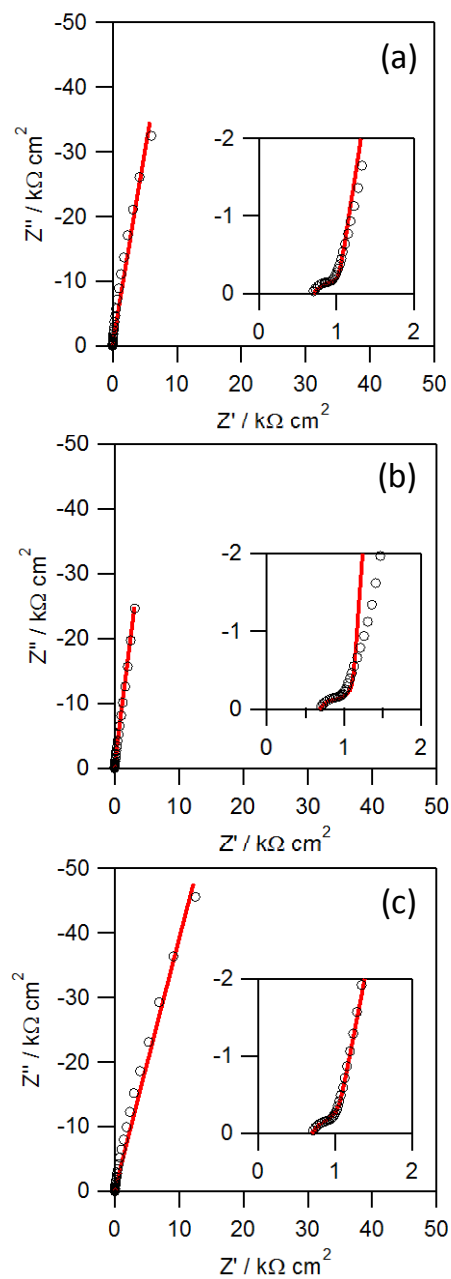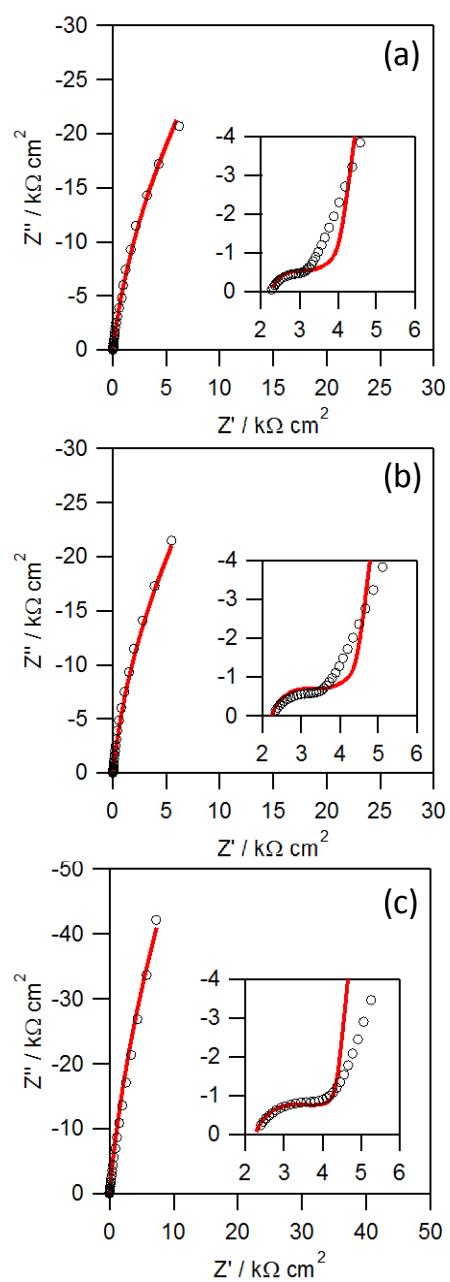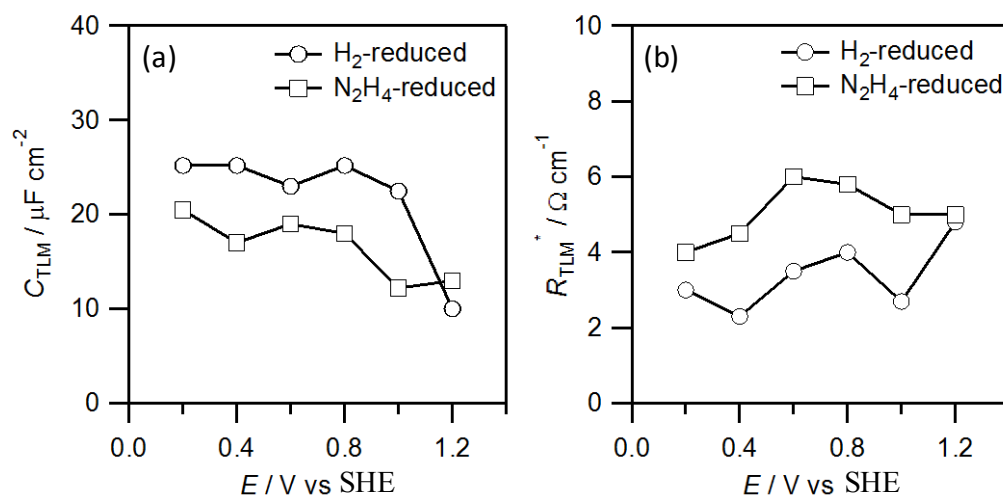
Figure 2-15. (a) C_{TLM} and (b) R_{TLM}^{*} in Na_2SO_4 from TLM simulation of (PDDA/

rGO)$_{10}$ reduced by H_2 or N_2H_4.
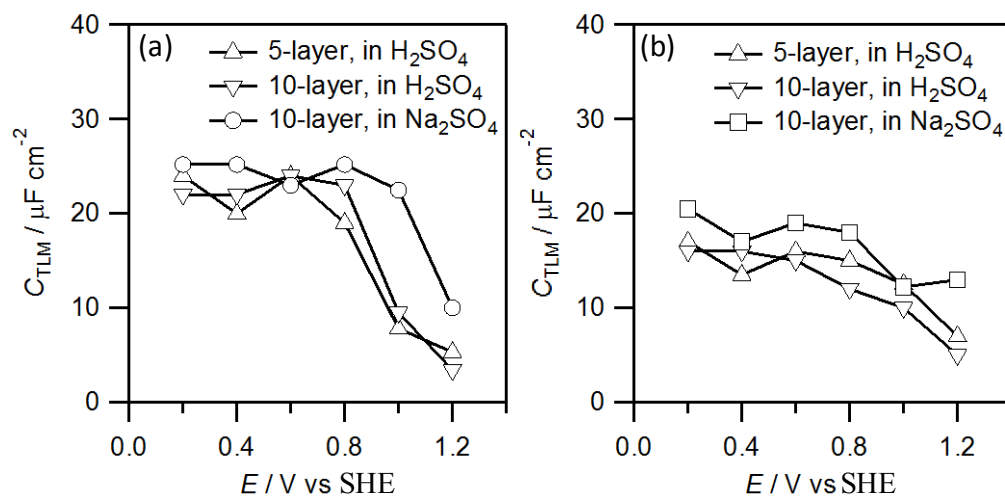
Figure 2-16. C_{TLM} from TLM-simulation of (PDDA/rGO)$_n$ (n=5, 10) reduced by (a) H$_2$

and (b) N$_2$H$_4$ in H$_2$SO$_4$ or Na$_2$SO$_4$.

Figure 2-17. C_{red} from TLM-simulation of $(PDDA/rGO)_n$ (n=5, 10) reduced by (a) H_2
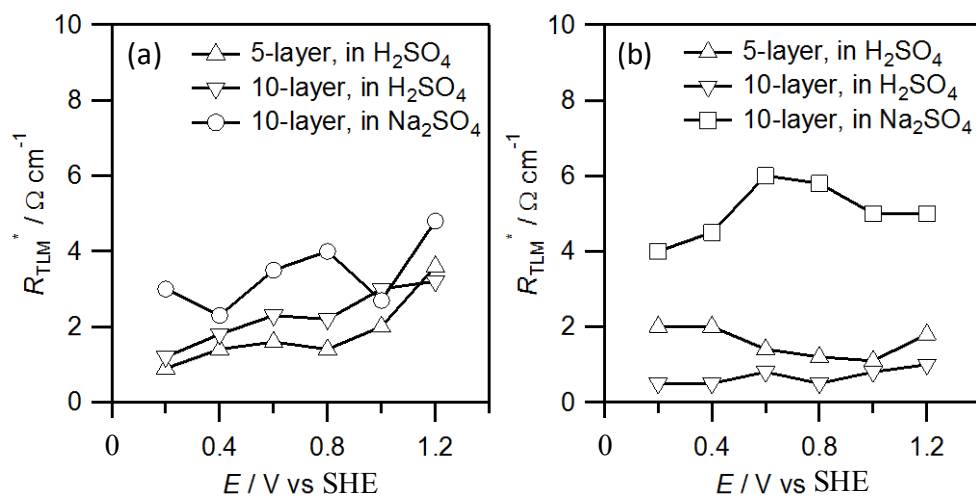
and (b) N_2H_4 in H_2SO_4.

Figure 2-18. R_{TLM}^{*} from TLM-simulation of $(PDDA/rGO)_n$ (n=5, 10) reduced by (a) H_2

and (b) N_2H_4 in H_2SO_4 or Na_2SO_4.

References

1. D. A. Brownson, D. K. Kampouris, and C. E. Banks, An overview of graphene in energy production and storage applications, *J. Power Sources*, **196** (2011), 4873.
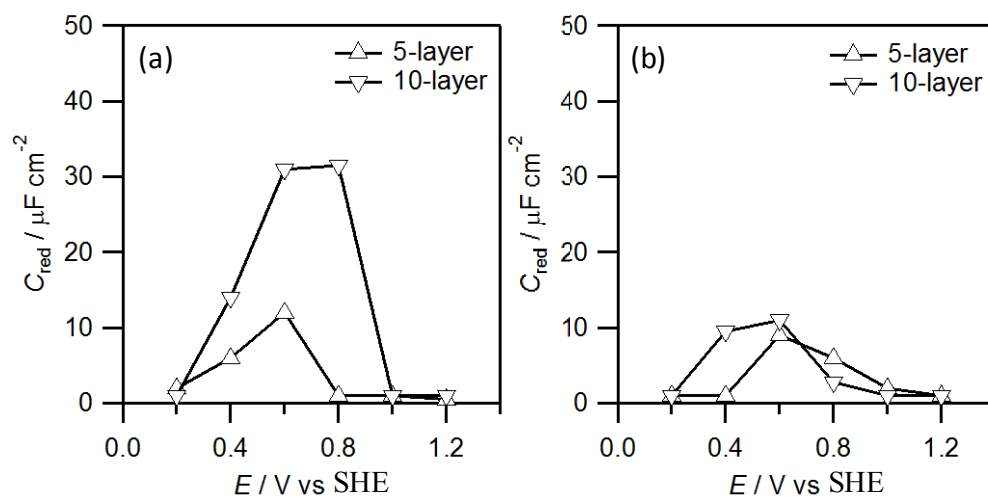
2. Y. Zhu, S. Murali, M. D. Stoller, K. J. Ganesh, W. Cai, P. J. Ferreira, A. Pirkle, R. M. Wallace, K. A. Cychosz, M. Thommes, D. Su, E. A. Stach, and R. S. Ruoff, Carbon-Based Supercapacitors Produced by Activation of Graphene. *Science*, **332** (2011), 1537.

3. H. Gomez, M. K. Ram, F. Alvi, P. Villalba, E. Stefanakos, and A. Kumar, Graphene-conducting polymer nanocomposite as novel electrode for supercapacitors. *J. Power Sources* **196** (2011), 4102.

4. A. K. Mishra and S, Ramaprabhu, Functionalized Graphene-Based Nanocomposites for Supercapacitor Application. *J. Phys. Chem. C* **115** (2011), 14006.

5. Z. Wu, G. Zhou, L. Yin, W. Ren, F. Li, and H. Cheng, Graphene/metal oxide composite electrode materials for energy storage. *Nano Energy*, **1** (2012), 107.

6. Q. Cheng, J. Tang, J. Ma, H. Zhang, N. Shinya, and L. Qin, Graphene and nanostructured MnO_2 composite electrodes for supercapacitors. *Carbon* **49** (2011), 2917.

7. S. Chen, J. Zhu, X. Wu, Q. Han, and X. Wang, Graphene Oxide–MnO_2 Nanocomposites for Supercapacitors. *ACS Nano* **4** (2010), 2822.

8. M. D. Stoller, S. Park, Y. Zhu, J. An, and R. S. Ruoff, Graphene-Based Ultracapacitors. *Nano Lett*, **8** (2008), 3498.

9. C. Liu, Z. Yu, D. Neff, A. Zhamu, and B. Z.Jang, Graphene-Based Supercapacitor with an Ultrahigh Energy Density. *Nano Lett.*, **10** (2010), 4863.

10. Y. Wang, Z. Shi, Y. Huang, Y. Ma, C. Wang, M. Chen, and Y. Chen, Supercapacitor Devices Based on Graphene Materials. *J. Phys. Chem. C*, **113** (2009)**,** 13103.

11. J. J. Yoo, K. Balakrishnan, J. Huang, V. Meunier, B. G. Sumpter, A. Srivastava, M. Conway, A. L. M. Reddy, J. Yu, R. Vajtai, and P. M. Ajayan, Ultrathin Planar Graphene Supercapacitors. *Nano Lett.*, **11** (2011)**,** 1423.

12. S. Zhang, Y. Li, and N. Pan, Graphene based supercapacitor fabricated by vacuum filtration deposition. *J. Power Sources*, **206** (2012), 476.

13. S. R. C. Vivekchand, C. S. Rout, K. S. Subrahmanyam, A. Govindaraj, and C. N. R. Rao, Graphene-based electrochemical supercapacitors. *J. Chem. Sci.*, **120** (2008), 9.

14. B. E. Conway, *Electrochemical Supercapacitor: Scientific Fundamentals and Technological Applications*, Kluwer: New York, 1999.

15. Y. Si, and E. T. Samulski, Exfoliated Graphene Separated by Platinum Nanoparticles. *Chem. Mater.*, **20** (2008), 6792.

16. J. Yan, T. Wei, B. Shao, F. Ma, Z. Fan, M. Zhang, C. Zheng, Y. Shang, W. Qian, and F. Wei, Electrochemical properties of graphene nanosheet/carbon black composites as electrodes for supercapacitors. *Carbon*, **48** (2010), 1731.

17. J. Sato, Y. Takasu, K. Fukuda, and W. Sugimoto, Graphene Nanoplatelets via Exfoliation of Platelet Carbon Nanofibers and Its Electrical double layer Capacitance. *Chem. Lett.*, **40** (2011), 44.

18. Z. Lei, T. Sakai, and W. Sugimoto, Lateral Size Effect on Electrochemical Capacitor Performance of Reduced Graphite Oxide Nanosheets. *Electrochemistry*, **80** (2013), 873.

19. Y. Li, M. Zijll, S. Chiang, and N. Pan, KOH modified graphene nanosheets for supercapacitor electrodes. *J. Power Sources*, **196** (2011), 6003.

20. M. M. Hantel, T. Kaspar, R. Nesper, A. Wokaun, R. Kotz, Partially reduced graphite oxide for supercapacitor electrodes: Effect of graphene layer spacing. *Electrochem. Commun.*, **13** (2011), 90.

21. L. L. Zhang, R. Zhou, and X. S. Zhao, Graphene-based materials as supercapacitor electrodes. *J. Mater. Chem.*, **20** (2010), 5983.

22. G. Decher, Fuzzy Nanoassemblies: Toward Layered Polymeric Multicomposites. *Science*, **277** (1997), 1232.

23. J. Shen, Y. Hu, C. Li, C. Qin, M. Shi, and M. Ye, Layer-by-Layer Self-Assembly of Graphene Nanoplatelets. *Langmuir*, **25** (2009)**,** 6122.

24. J. S. Park, S. M. Cho, W. J. Kim, J. Park, and P. J. Yoo, Fabrication of Graphene Thin Films Based on Layer-by-Layer Self-Assembly of Functionalized Graphene Nanosheets. *ACS Appl. Mater. Interfaces*, **3** (2011)**,** 360.

25. D. Yu, and L. Dai, Self-Assembled Graphene/Carbon Nanotube Hybrid Films for Supercapacitors. *J. Phys. Chem. Lett.*, **1** (2010), 467.

26. A. K. Sarker, and J. D. Hong, Layer-by-Layer Self-Assembled Multilayer Films Composed of Graphene/Polyaniline Bilayers: High-Energy Electrode Materials for

Supercapacitors. *Langmuir*, **28** (2012), 12637.

27. T. Szabo, A. Szeri, and I. Dekany, Composite graphitic nanolayers prepared by self-assembly between finely dispersed graphite oxide and a cationic polymer. *Carbon*, **43** (2005), 87.

28. P. Ni, H. Li, M. Yang, X. He, Y. Li, and Z. H. Liu, Study on the assembling reaction of graphite oxide nanosheets and polycations. *Carbon*, **48** (2010), 2100.

29. X. Zhao, Q. Zhang, Y. Hao, Y. Li, Y. Fang, and D. Chen, Alternate Multilayer Films of Poly(Vinyl alcohol) and Exfoliated Graphene Oxide Fabricated via a Facial Layer-by-Layer Assembly. *Macromolecules*, **43** (2010), 9411.

30. W. S. Hummers, and R. E. Offeman, Preparation of Graphitic Oxide. *J. Am. Chem. Soc.*, **80** (1958), 1339.

31. M. Itagaki, S. Suzuki, I. Shitanda, K. Watanabe, and H. Nagazawa, Impedance analysis on electrical double layer capacitor with transmission line model. *J. Power Sources*, **164** (2007), 415.

32. M. Itagaki, M. Igarashi, and K. Watanabe, Electrochemical Impedance of the Various Crevice Electrodes – Computer Simulation by Using Matrix. *Electrochemistry*, **70** (2002), 686.

33. D. Qu, and H. Shi, Studies of activated carbons used in double-layer capacitors. *J. Power Sources*, **74** (1998)**,** 99.

34. R. de Levie. On porous electrodes in electrolyte solutions—IV. *Electrochim. Acta*, **9**, (1964)**,** 1231.

Chapter 3

Lateral Size Effect on Electrochemical Capacitor Performance of Reduced Graphite Oxide Nanosheets

3.1 Introduction

Graphene has attracted increased interest due to its high theoretical surface area, electron mobility and stability,[1,2] in particular for electrochemical applications such as fuel cells and electrochemical capacitors.[3] While a number of methods have been developed for the preparation of graphene,[4-10] the scalable and low cost approach using a sequential oxidation-exfoliation-reduction procedure has attracted most attention. Specific capacitance of graphene (reduced graphite oxide nanosheet) electrodes prepared by this approach ranges from 100 to 250 F g^{-1}. The dispersed capacitance values is due at least in part to the difference in synthetic procedures, including the starting materials used, degree of exfoliation, degree of reduction, etc. The lateral size of reduced graphite oxide sheets is expected to be one of the factors affecting the electrochemical properties. It has been reported that the specific capacitance of the edge plane of graphite (c.a. 50-70 μF cm^{-2}) is much higher than its basal plane (~3 μF cm^{-2}).[11] It was reported that reduced graphite oxide nanosheets derived from platelet carbon nanofibers (PCNFs) with average diameter of 150 nm gives approximately 60% higher specific capacitance compare to that derived from natural graphite with average size of ~3 μm.[12] Although reduced graphite oxide nanosheets (rGOns) prepared by this approach gives nanosheets with well defined size, the nanosheet size is determined by the nanofiber diameter, which is not easily controlled. Also, the synthetic method is not easily scalable due to the cost of the starting material and low yield.

In this chapter, reduced graphite oxide nanosheets with different lateral size was

prepared from the same graphite as starting material, and the electrochemical capacitor behavior was studied in an attempt to clarify the relationship between the nanosheet size and capacitor performance. The lateral size of graphite oxide nanosheets was manipulated by controlled treatment of graphite oxide nanosheet colloids.

3.2 Experimental

Graphite oxide was prepared following the Hummers method[13] using a graphite powder with average particle size of 4 μm (Z-5F, ITO GRAPHITE Co., Ltd.) as the starting material. Graphite oxide was dispersed in ultrapure water (> 18 M• cm), then exfoliated to graphite oxide nanosheets assisted by mild ultrasonic treatment with a common ultrasonic bath. Non-exfoliated graphite oxide was removed by centrifugation at 2000 rpm for 30 min, affording a homogeneous brownish colloid.

The as-prepared GOns colloid was subjected to high power ultrasonic treatment with frequency of 20 kHz (VCX-750, Sonic & Materials, Inc., 750 W) for 30 min to breakdown the lateral size of GOns in the colloid. Further downsizing was conducted by ultrasonic treatment of the 20 kHz-treated colloid with higher frequency (950 kHz, Mitsui Electric Co., Ltd., 300 W) for 20 minutes.

The lateral size of individual GOns was evaluated using AFM (SPM-400, Seiko Instruments Inc.). Sub-monolayer of GOns was deposited on Si by dipping the substrate into the colloid for 10 min, followed by mild washing with ultrapure water and drying under ambient conditions. The area (A) and perimeter (P) of individual GOns in the

atomic force microscopic images were measured and the equivalent diameter (D_e) was calculated by:

$$D_e = \frac{4 \times A}{P}$$

The size adjusted GOns colloids were dropped on a polished glassy carbon electrode, dried at 60 °C, and reduced at 200 °C for 2 hours under H_2/Ar (5/95) flow, or with $N_2H_4 \cdot H_2O$ at 60 °C for 24 hours. Cyclic voltammetry was conducted using a HZ-5000 system (Hokuto Denko Corp.) in 0.5 M H_2SO_4 or Na_2SO_4.

X-ray diffraction (XRD) was conducted on RINT2550H/PC (Rigaku Corp.) with the colloids dropped on glass plate and dried at 60 °C. FE-SEM was observed using a Hitachi S-5000 system. The specific surface area of rGOns powder was measured by nitrogen adsorption at 77 K with Belsorp-18 (BEL Japan Inc.). Thermogravimetric analysis (TGA-50, Shimadzu Corp.) was conducted under H_2/Ar (5/95) flow to estimate the oxygen content of the sample. X-ray photoelectron spectrometry was acquired with AXIS-ULTRA DLD (Kratos Analytic Ltd.).

3.3 Results and Discussion

Figure 3-1 shows the AFM images of GOns with different ultrasonic treatment. All of the nanosheets had thickness of less than 1 nm, indicating complete exfoliation of graphite oxide to individual GOns. GOns had very few overlapping and no folding, making it proper for evaluation of the nanosheet size. The calculated D_e were 921, 373, 277 nm for as-prepared, 20 kHz-treated and 950 kHz-treated GOns, respectively. The

samples will be denoted GOns(920nm), GOns(370nm) and GOns(280nm) hereafter.

Figure 3-2 (a) and (b) shows typical cyclic voltammograms in 0.5 M H_2SO_4 of GOns(920nm), GOns(370nm) and GOns(280nm) reduced by H_2 or N_2H_4. The reduced sample will be denoted rGOns(920nm), rGOns(370nm) and rGOns(280nm) hereafter. Redox peaks at ~0.6 V were observed, suggesting the presence of oxygen-containing surface functionalities. For the H_2-reduced series, the specific capacitance at 2 mV s^{-1} was 197, 214 and 242 F g^{-1} for rGOns(920nm), rGOns(370nm) and rGOns(280nm), respectively. The N_2H_4-reduced samples showed lower capacitance of 150, 157 and 192 F g^{-1} for rGOns(920nm), rGOns(370nm) and rGOns(280nm), respectively. In order to exclude the influence from redox-related capacitance, cyclic voltammetry was conducted in 0.5 M Na_2SO_4 (Fig. 3-2 (c)). The specific capacitance for the H_2 reduced samples were 185, 193 and 205 F g^{-1} for rGOns(920nm), rGOns(370nm) and rGOns(280nm), respectively. An increase in specific capacitance with the decrease of nanosheet size was observed even without contribution from pseudo-capacitance (purely electrical-double layer charging). The increase in electrical-double layer capacitance should be attributed to a higher electrochemically active surface area for the rGOns with smaller lateral size, and will be discussed in detail later. It is noted that over 98% of the initial capacitance was maintained even after potential cycling tests of rGOns(280nm) in 0.5 M H_2SO_4 at 50 mV s^{-1} for 5000 cycles (Fig. 3-3).

The relative ratio of carbon with C-C, C-O and C(=O)-O bonding based on XPS for the samples before reduction (Fig. 3-4) are shown in Table 3-1. As the sheet size

decreases, a decrease in the relative ratio of C-O bonds is observed, which is correlated with an increase in the ratio of C(=O)-O bonds. Also the O/C ratio for the samples reduced by both methods was calculated based on XPS (Figure 3-5) and is summarized in Table 3-2. H_2-reduced rGOns has a higher O/C ratio compared to the N_2H_4-reduced samples, which explains the higher contribution from redox-related pseudo-capacitance observed for the H_2-reduced rGOns series (see Fig. 3-2). Another point is that more oxygen was found in samples with smaller sheet size. Again, this is in accord with the higher contribution from redox-related pseudo-capacitance observed for the rGOns with smaller nanosheet size.

Figure 3-6 shows the XRD patterns of the samples before and after reduction with H_2 and N_2H_4. As the nanosheet size of GOns decreases, the inter-layer distance increases from 0.73 to 0.83 nm. The peak is also weaker for smaller size GOns, suggesting that the smaller size GOns may be more loosely stacked and disordered than the larger size GOns. Reduced samples show very weak and broad peaks at $2\theta \bullet 25°$ ($d \bullet 0.36$ nm), signifying that rGOns is more disordered and heterogeneous than GOns. The peak at $d \bullet 0.36$ nm in rGOns is slightly weaker for rGOns with smaller size. This may suggest that rGOns(370nm) and rGOns(280nm) has a more irregular lamellar structure compared to rGOns(920nm). In fact, SEM images of the H_2 reduced samples (Figure 3-7) seems to show rGOns(920nm) with a more smooth surface morphology than rGOns(370nm) and rGOns(280nm).

The adsorption/desorption isotherms and pore size distribution curves are shown in

Figure 3-8. The BET surface area increased as the nanosheet size decreased; 143, 247 and 293 $m^2 g^{-1}$ for H_2-reduced rGOns(920nm), rGOns(370nm) and rGOns(280nm), respectively. rGOns(920nm) has a sharp pore size distribution centered at ~1.7 nm. The main peak in the pore size distribution is shifted to slightly larger region (~1.9 nm) for rGOns(370nm) and rGOns(280nm). While most of the pores for rGOns(920nm) are below r_p=2.5 nm, rGOns(370nm) and rGOns(280nm) have medium to large-size mesopores. The results agree with the XRD and SEM analysis that showed more disorder for the smaller-sized rGOns.

Based on the above findings, the reason for the increase in specific capacitance of rGOns with decreasing nanosheet size is discussed. It was reported that the edge of graphite oxide is mainly COOH, while COH and C-O-C is present on the basal plane.[14] When GOns is broken down by ultrasonic treatment, a large number of C- dangling bonds should be created on the newly generated edges. These highly active dangling bonds are easily oxidized to COOH, leading to an overall decrease in C-O bonding and an increase in COOH with decreasing nanosheet size. Thus, a higher content of surface functional groups will remain on smaller nanosheets, leading to higher pseudo-capacitance.

Table 3-3 summarizes the specific capacitance per unit surface area of H_2 reduced samples in H_2SO_4 and Na_2SO_4. The area-specific capacitance is much higher than the often observed typical value of ~20 $\mu F cm^{-2}$.[15, 16] This is tentatively attributed partially to the possible difference in the stacking state of rGOns at the dry (when the specific

surface area was measured by N_2 adsorption/desorption) and wet (when the electrode was immersed in electrolyte for electrochemical measurements) states, and partially to the narrow pore size distribution of rGOns. In fact, the area-specific capacitance decreases with decreasing nanosheet size, which is in agreement with the wider pore size distribution for rGOns(370nm) and rGOns(280nm). Although the gravimetric capacitance increases as the nanosheet size decreases, the area-specific capacitance is smaller for smaller-sized nanosheets in both H_2SO_4 and Na_2SO_4 electrolytes. This seems at first glance to contradict with the assumption that the edge sites have higher area-specific capacitance than the planes. However, as mentioned above, the porosity must also be taken into consideration.

3.4 Conclusions

The specific capacitance of graphite oxide nanosheets reduced by hydrogen or hydrazine was successfully enhanced by reducing the lateral size of the nanosheets before reduction with high power ultrasonic treatment. A high specific capacitance of 240 F g^{-1} in H_2SO_4 and 205 F g^{-1} in Na_2SO_4 at 2 mV s^{-1} was achieved for H_2-reduced graphite oxide nanosheets with an equivalent diameter of 280 nm. The unusually high capacitance per unit surface area of ~100 μF cm^{-2} is expected to lead to a higher volumetric capacitance than conventional activated carbons.

The sheet size-effect on electrochemical capacitance of graphene nanosheets could be attributed to:

First, the concentration of charge on graphene edge or corners[17] as well as more

space for the edge carbon atoms to accommodate counter ions compared to that at basal plane (Figure 3-9), as a result, every carbon atom at the edges or corners can attract more counter ions compare to those at the basal plane;

Second, more oxygen functional groups tend to be remained on edges or corners, leading to more pseudo-capacitance;

And third, The nanosheets with smaller size would be more difficult to densely restack compare to larger nanosheets, leading to a relatively high surface area for the smaller sheets.

Table 3-1. The ratio of the different C species based on XPS for GOns (non-reduced) with different size.

sample	Ratio of species (%)		
	C-C	C-O	C(=O)-O
GOns(920nm)	53	34	13
GOns(370nm)	54	29	17
GOns(280nm)	54	26	20

Table 3-2. O/C ratio for rGOns(920nm), rGOns(370nm) and rGOns(280nm) reduced by H_2 and N_2H_4.

Reductant	Sample	O/C
	rGOns(920nm)	15/85
H_2	rGOns(370nm)	21/79
	rGOns(280nm)	27/73
	rGOns(920nm)	10/90
N_2H_4	rGOns(370nm)	12/88
	rGOns(280nm)	13/87

Table 3-3. Area-specific capacitance of H_2 reduced sample in different

electrolytes.

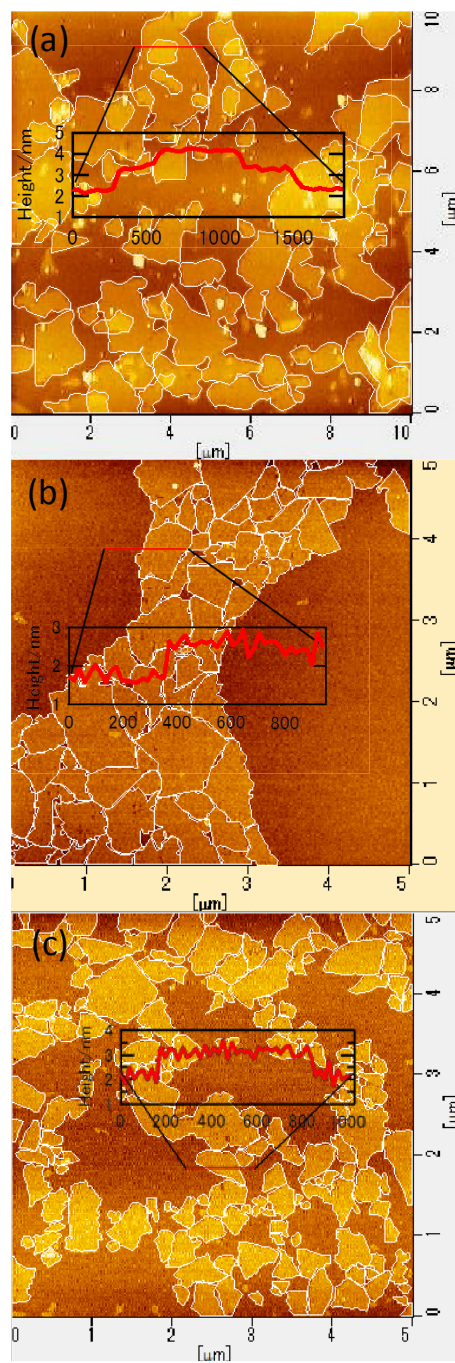| Sample	Specific capacitance / $\mu F\ cm^{-2}$	
	0.5 M H_2SO_4	0.5 M Na_2SO_4
rGOns(920nm)	138	129
rGOns(370nm)	87	78
rGOns(280nm)	83	70

Figure 3-1. AFM images of (a) GOns(920nm), (b) GOns(370nm) and (c) GOns(280nm) for size analysis.
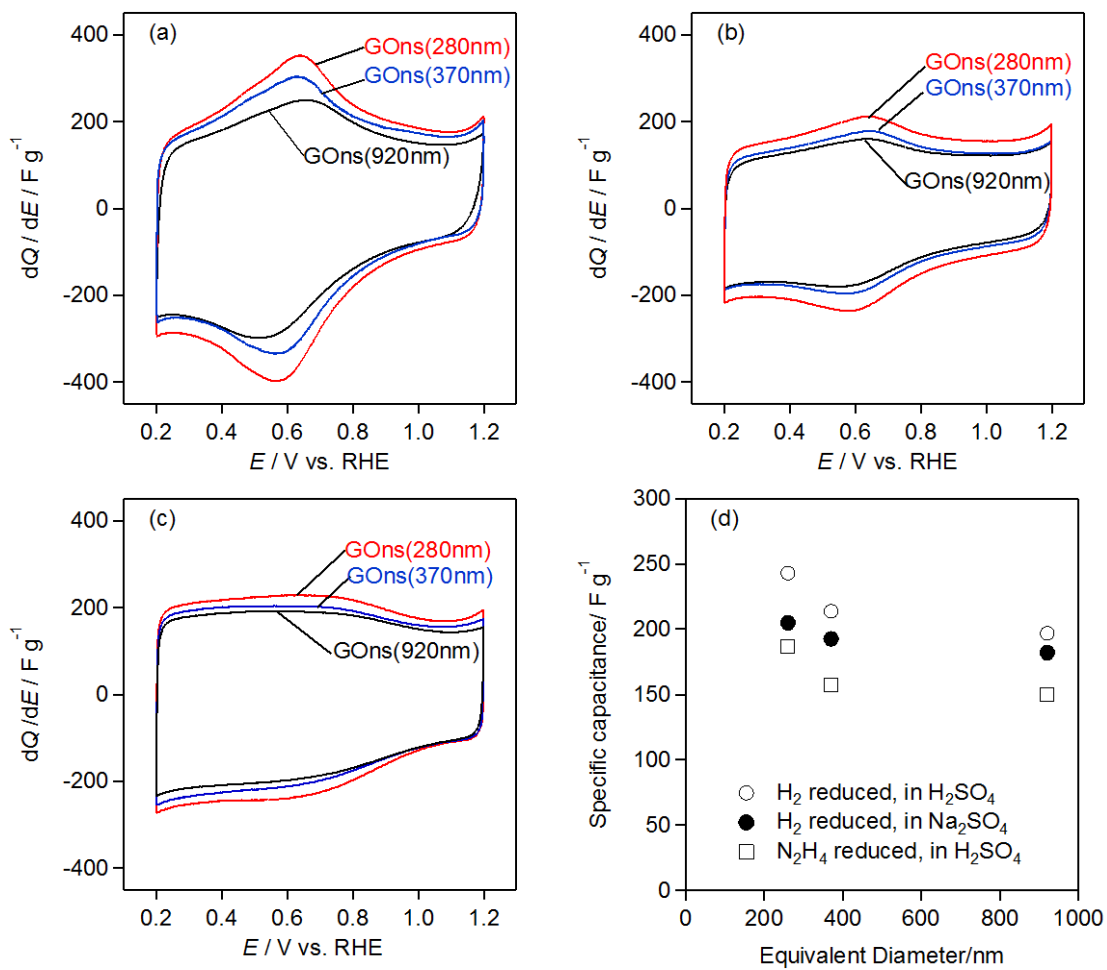
Figure 3-2. Cyclic voltammograms of (a) H_2- and (b) N_2H_4-reduced samples in 0.5 M H_2SO_4, (c) H_2-reduced sample in 0.5 M Na_2SO_4, at 20 mV s^{-1}. (d) The specific capacitance as a function of average equivalent diameter of rGOns taken from (a)-(c).
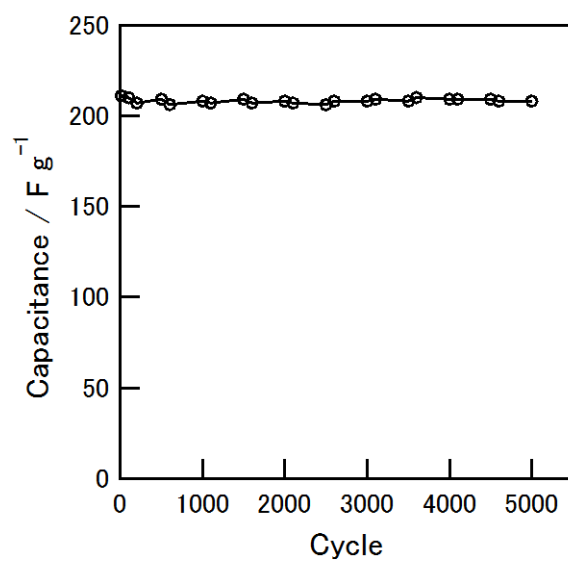
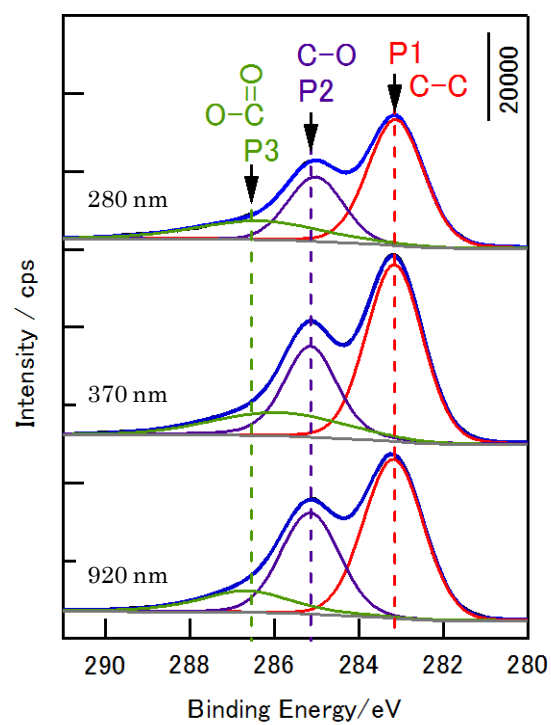Figure 3-3 Specific capacitance of rGOns(280nm) in H_2SO_4 for 5000 CV cycles.

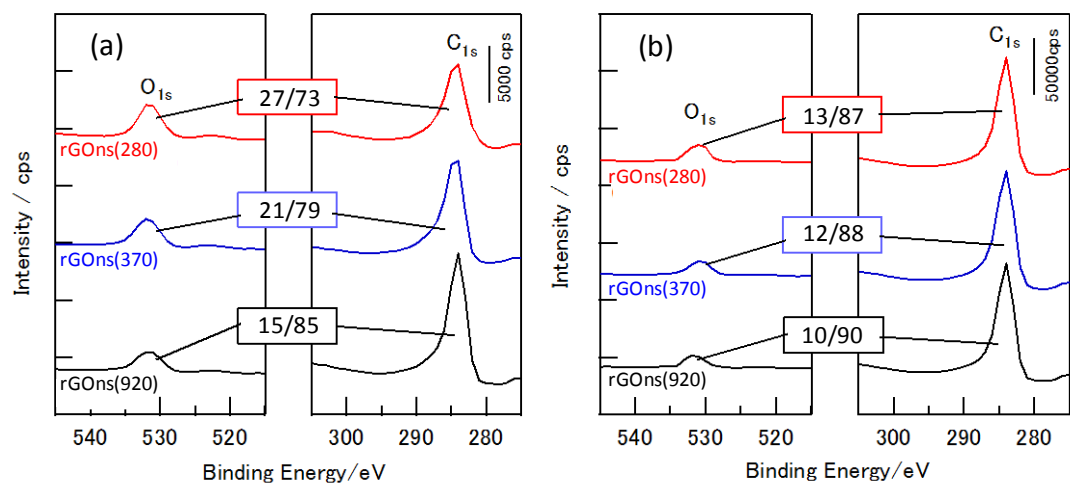Figure 3-4. X-ray photoelectron spectroscopy for samples with different lateral size before reduction.

Figure 3-5. O/C atomic ratio for reduced rGOns(920), rGOns(370) and rGOns(280) reduced by (a) H_2 and (b) N_2H_4.
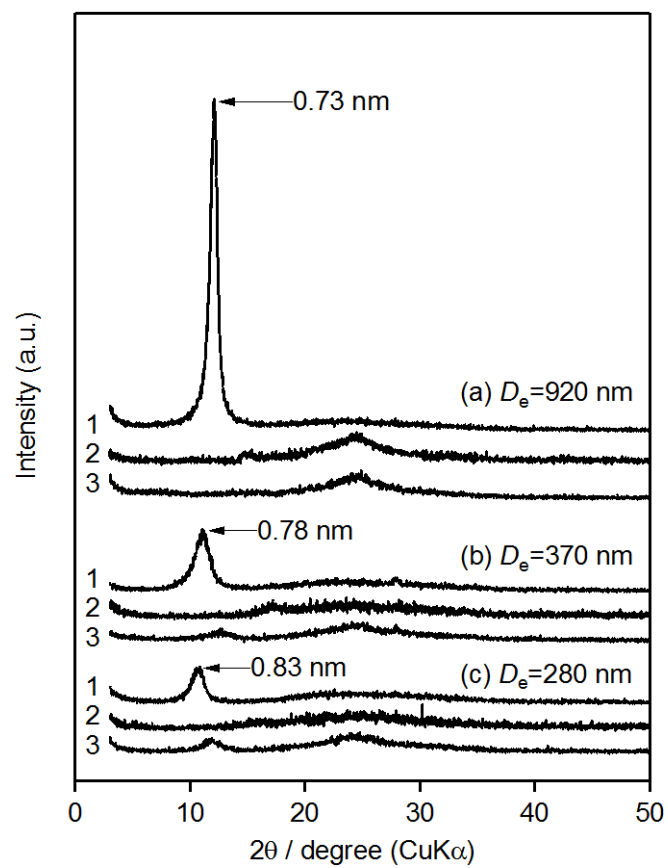
Figure 3-6. XRD patterns for (1) non-reduced, (2) H_2-reduced, and (3) N_2H_4-reduced

samples of GOns with D_e=(a) 920nm, (b) 370nm, and (c) 280nm.
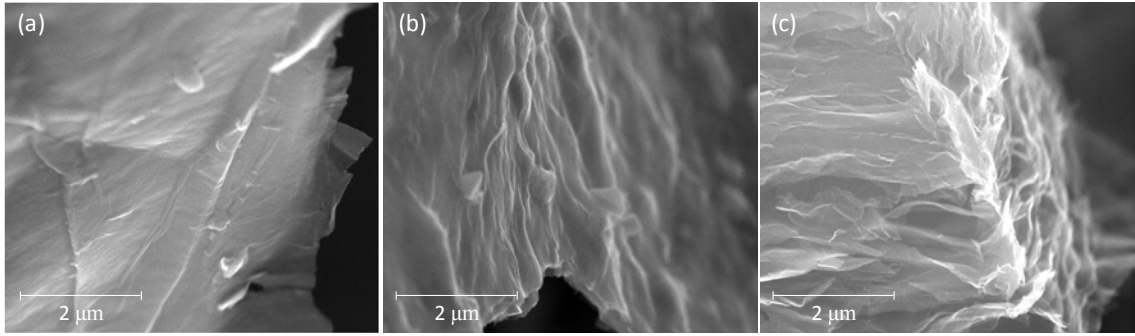
Figure 3-7. FE-SEM images of H_2-reduced (a) rGOns(920nm), (b) rGOns(370nm), and (c) rGOns(280nm).
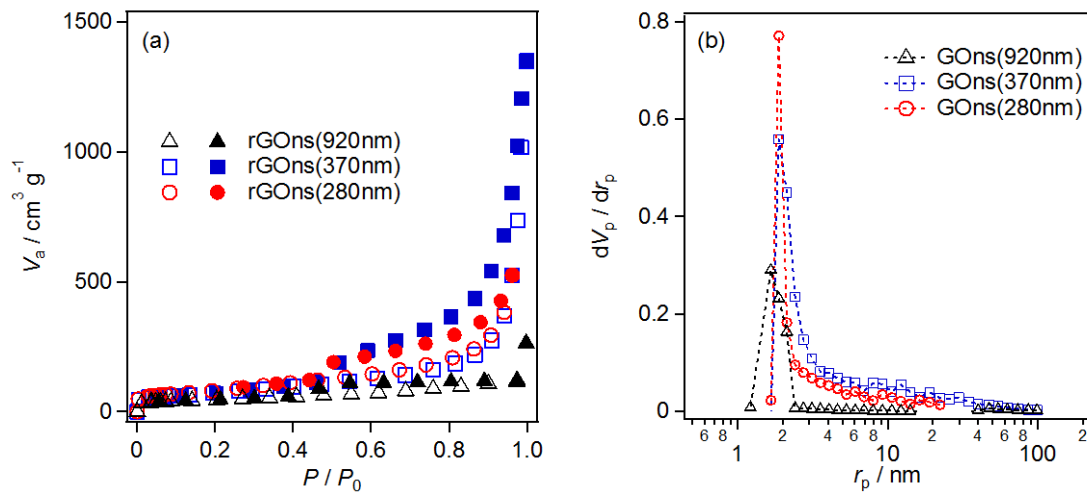
Figure 3-8. (a) Adsorption (open plots)/desorption (filled plots) isotherms and (b) pore size distribution curves (BJH plot) for H_2-reduced rGOns with D_e=920, 370, and 280 nm.

Charged graphene sheet with higher
charge density near edge

Counter Ion

Edge

Basal plane

Specific capacitance

Position on graphene nanosheet

Figure 3-9. Schematic for charge-concentration and space accommodation effect for

edge atoms of graphene sheets.

References

1. A. K. Geim and K. S. Novoselov, The rise of graphene. *Nat. Mater.*, **6** (2007), 183.

2. K. I. Bolotin, K. J. Sikes, Z. Jiang, M. Klima, G. Fudenberg, J. Hone, P. Kim, and H. L. Stormer, Ultrahigh electron mobility in suspended graphene. *Solid State Commun.*, **146** (2008), 351.
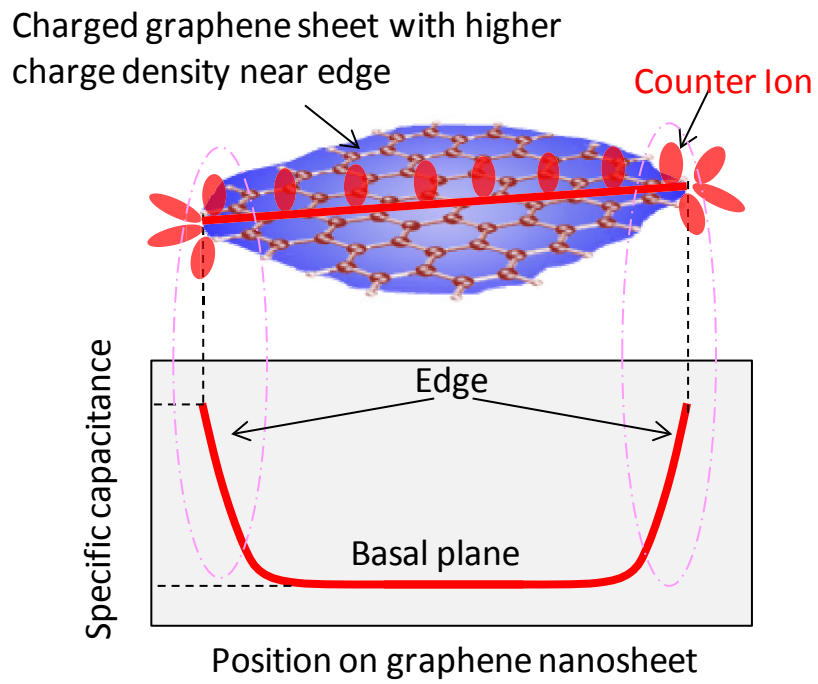
3. D. A. Brownson, D. K. Kampouris, and C. E. Banks, An overview of graphene in energy production and storage applications. *J. Power Sources*, **196** (2011), 4873.

4. K. S. Novoselov, A. K. Geim, S. V. Morozov, D. Jiang, Y. Zhang, S. V. Dubonos, I. V. Grigorieva, and A. A. Firsov, Electric Field Effect in Atomically Thin Carbon Films. *Science*, **306** (2004), 666.

5. X. Li, W. Cai, J. An, S. Kim, J. Nah, D. Yang, R. Piner, A. Velamakanni, I. Jung, E. Tutuc, S. K. Banerjee, L. Colombo, and R. S. Ruoff, Large-Area Synthesis of High-Quality and Uniform Graphene Films on Copper Foils. *Science*, **324** (2009), 1312.

6. S. Bae, H. Kim, Y. Lee, X. Xu, J. Park, Y. Zheng, J. Balakrishnan, T. Lei, H. R. Kim, Y. I. Song, Y. J. Kim, K. S. Kim, B. Ozyilmaz, J. H. Ahn, B. H. Hong, and S. Iijima, Roll-to-roll production of 30-inch graphene films for transparent electrodes. *Nat. Nanotechnol.*, **5** (2010), 574.

7. M. D. Stoller, S. Park, Y. Zhu, J. An, and R. S. Ruoff, Graphene-Based Ultracapacitors. *Nano Lett.*, **8** (2008), 3498.

8. Y. Zhu, S. Murali, M. D. Stoller, A. Velamakanni, R. D. Piner, and R. S. Ruoff,

Microwave assisted exfoliation and reduction of graphite oxide for ultracapacitors. *Carbon*, **48** (2010), 2118.

9. Z. Lin, Y. Liu, Y. Yao, O. J. Hildreth, Z. Li, K. Moon, and C. Wong, Superior Capacitance of Functionalized Graphene. *J. Phys. Chem. C*, **115** (2011), 7120.

10. Y. Wang, Z. Shi, Y. Huang, Y. Ma, C. Wang, M. Chen, and Y. Chen, Supercapacitor Devices Based on Graphene Materials. *J. Phys. Chem. C*, **113** (2009), 13103.

11. J. Randin and E. Yeager, Differential Capacitance Study of Stress‐Annealed Pyrolytic Graphite Electrodes. *J. Electrochem. Soc.*, **118** (1971), 711.

12. J. Sato, Y. Takasu, K. Fukuda, and W. Sugimoto, Graphene Nanoplatelets via Exfoliation of Platelet Carbon Nanofibers and Its Electrical double layer Capacitance. *Chem. Lett.*, **40** (2011), 44.

13. W. S. Hummers and R. E. Offeman, Preparation of Graphitic Oxide. *J. Am. Chem. Soc.*, **80** (1958), 1339.

14. A. Lerf, H. He, M. Forster, and J. Klinowski, Structure of Graphite Oxide Revisited. *J. Phys. Chem. B*, **102** (1998), 4477.

15. B. E. Conway, *Electrochemical Supercapacitor: Scientific Fundamentals and Technological Applications*, Kluwer: New York, 1999.

16. J. Xia, F. Chen, J. Li, and N. Tao, Measurement of the quantum capacitance of graphene. *Nat. Nanotechnol.*, **4** (2009), 505.

17. Z. Wang and R. Scharstein, Electrostatics of Graphene: Charge Distribution and Capacitance. *Chem. Phys. Lett.*, **489**, 229 (2010).

Chapter 4

Conclusions

This thesis focuses on the fundamental scientific understanding of graphene-based material for electrochemical charge storage applications. First, the basic electrochemical behavior of graphene-like sheets were investigated by fabricating lamellar nano-architectures composed of reduced graphene oxide spaced by polymer chains using layer-by-layer self-assembly followed by reduction with H_2 or N_2H_4. Electrochemical analysis with cyclic voltammetry and electrochemical impedance spectroscopy indicates a full utilization of rGO layers for charge storage. The electrical double layer capacitance was evaluated with neutral Na_2SO_4, while pseudo-capacitance attributed to oxygen functionalities was analyzed in H_2SO_4. The results show that the electrical double layer capacitance of rGO is roughly 20-30 μF cm^{-2}, and it is correlated to the ionic conductivity and hydrophobility in the polymer-spaced gaps, which affects the degree of reduction of rGO. The H_2-reduced samples (O/C=0.21) tend to have higher electrical double layer capacitance compared to N_2H_4-reduced counterparts (O/C=0.10) due to its higher hydrophilicity. On the other hand, the pseudo-capacitance increases proportionally with the increase of oxygen functionality groups.

Secondly, the electrochemical performance of graphene-like sheets with different lateral size was investigated. The specific capacitance of graphene oxide sheets reduced by hydrogen or hydrazine was successfully enhanced by reducing the lateral size of the nanosheets before reduction with high power ultrasonic treatment. The increase in capacitance with the decrease in lateral size is attributed to at least two causes, the higher specific surface area of reduced graphite oxide nanosheets with smaller

nanosheet size, and the edge-induced increase of functional groups. A high specific capacitance of 240 F g^{-1} in H$_2$SO$_4$ and 205 F g^{-1} in Na$_2$SO$_4$ at 2 mV s^{-1} was achieved for H$_2$-reduced graphite oxide nanosheets with an equivalent diameter of 280 nm. The unusually high capacitance per unit surface area of ~100 μF cm^{-2} is expected to lead to a higher volumetric capacitance than conventional activated carbons.

List of Terms and Definitions

Anode: The electrode through which positive electric charge flows into a polarized electrical device.

Cathode: The electrode from which a current leaves a polarized electrical device.

Counter electrode: An electrode used in a three-electrode electrochemical cell for voltammetric analysis as the path of an electrical current.

Cyclic voltammetry: A type of potentiodynamic electrochemical measurement. In a cyclic voltammetry experiment the potential of working electrode is ramped linearly versus time like linear sweep voltammetry and the response current to be recorded for analysis.

Electric double layer: A structure of two parallel layers of charge surrounding the surface of an object when it is exposed to a fluid. The first layer is a layer of charge on the surface of the object (the surplus or deficiency of electron). The second layer is composed of ions attracted to the surface charge via coulomb force.

Electrochemical capacitor: Also as known to be *supercapacitor* or *ultracapacitor*. Is a class of capacitive device based on electrochemistry. Mainly include electric double layer capacitor based on electric double layer and pseudo-capacitor based on fast redox reactions.

Electrochemical impedance analysis: An electrochemical analysis approach in which

an AC potential to be applied on an electrochemical cell with the current through the cell being measured, then the impedance of the electrochemical cell to be analyzed. It is a powerful tool for kinetic analysis of electrochemical systems.

Electrode: An electrical conductor used to make contact with a non-electronic-conductive part of a circuit (e.g. an electrolyte or vacuum).

Electrolyte: A substance that ionizes when dissolved in suitable ionizing solvents such as water or organic solvents. Electrolyte solutions are usually ionic-conductive liquid formed when a salt is dissolved into a solvent, but there are also ionic-conductive electrolytes in solid state.

Graphene: A 2-dimensional crystal with a monolayer of carbon atoms tightly packed into a honeycomb lattice with a C-C bond of 142 pm.

Graphene oxide: A 2-dimensional sheet with a monolayer of graphene with part of carbon atoms being oxidized, include various contents of oxygen and hydrogen atoms.

Graphite oxide: A compound of carbon, oxygen, and hydrogen in variable ratios, usually obtained by treating graphite with strong oxidizers, basically the layered structure of graphite is remained with the interlayer distance expanded.

Pseudo-capacitance: A capacitive-like capacitance (store of charge) derived from reversible faradaic redox reactions near the surface of electrode in an electrochemical capacitor.

Redox reaction: Couples of electrochemical reducing and oxidizing reactions occurs in an electrochemical system.

Reduced graphene oxide: The product of graphene oxide after reduced by thermal treatment or chemical treatments using chemicals such as hydrazine.

Reference electrode: An electrode used in a three-electrode electrochemical cell for the determining of potential of the working electrode. The reference electrode has to possess a well-known and stable electrode potential. Electrodes such as silver chloride electrode (Ag/AgCl), saturated calomel electrode (SCE) or standard hydrogen electrode (SHE) are commonly used as reference electrodes in practice.

Acknowledgment

There are many people that I would like to acknowledge for their help during my studies for this thesis. First, I thank my advisor, Prof. Wataru Sugimoto, without the exceptionally thoughtful guidance and advices from whom, I could never have finished my study. It is a great privilege to be able to discuss research with such a distinguished scientist. As a foreign student, I was supported in both research and personal life by many of the professors, students and staff in our group, all of them are greatly appreciated for their kind support.

I also got a lot of support or advice from professors or experts in the community of electrochemistry or material science outside of the campus. Prof. Toshio Sakai from Faculty of Engineering, Shinshu University supported me on ultrasonic treatment of my samples. Prof. Masayuki Itagaki from Tokyo University of Science gave me kind support on the transmission line model simulation of electrochemical impedance. Here I thank all of them for all the great support.

I would like to thank the financial support provided by the Global COE and the Grants for Excellent Graduate Schools, MEXT, Japan.

Finally, I would like to thank my family, especially my wife, who always supports me at whatever hard times.

<div style="text-align: right">

Zhongwei LEI

</div>